Article:

Wang, Y., Wang, W. and Susmel, L. orcid.org/0000-0001-7753-9176 (2021) Constant/variable amplitude multiaxial notch fatigue of additively manufactured AISI 316L. International Journal of Fatigue, 152. 106412. ISSN 0142-1123

https://doi.org/10.1016/j.ijfatigue.2021.106412

Constant/variable amplitude multiaxial notch fatigue of additively manufactured AISI 316L

Yingyu Wang[1], Wenxuan Wang[1] and Luca Susmel[2]

[1]Key Laboratory of Fundamental Science for National Defense-Advanced Design Technology of Flight Vehicle, Nanjing University of Aeronautics and Astronautics, Nanjing, 210016, China
[2]Department of Civil and Structural Engineering, the University of Sheffield, Sheffield S1 3JD, UK

Corresponding Author: Prof. **Luca Susmel**
Department of Civil and Structural Engineering
The University of Sheffield, Mappin Street, Sheffield, S1 3JD, UK
Telephone: +44 (0) 114 222 5073
Fax: +44 (0) 114 222 5700
e-mail: l.susmel@sheffield.ac.uk

ABSTRACT

A specific design approach is formulated to design notched components of additively manufactured AISI 316L against constant/variable amplitude multiaxial fatigue loading. The accuracy of the proposed approach was checked against experimental results generated by testing, under constant/variable amplitude biaxial loading, plain/notched cylindrical specimens of 3D-printed AISI 316L. Specific experimental trials were run to investigate also the effect of out-of-phase angles equal to 90º and superimposed static stresses. The sound agreement between experimental results and predictions confirms that the proposed approach can be used safely in situations of practical interest to perform multiaxial fatigue assessment of notched additively manufactured components.

Keywords: Additive manufacturing, multiaxial fatigue, variable amplitude, critical plane, critical distance.

Nomenclature

A, B	material fatigue constants in the L_M vs. N_f relationship
D	total damage sum
D_{cr}	critical value of the damage sum
$D_{cr,av}$	average experimental value of the critical value of the damage sum
$D_{cr,exp}$	experimental critical value of the damage sum
E	Young's modulus
f	frequency of the applied loading
k	negative inverse slope of the fully-reversed uniaxial fatigue curve
k_0	negative inverse slope of the fully-reversed torsional fatigue curve
$k_\tau(\rho_{eff})$	negative inverse slope of the modified Wöhler curve
L	critical distance in the high-cycle fatigue regime
L_M	critical distance in the finite life regime
m	mean stress sensitivity index
n_i	i-th fatigue cycle
N_A	reference number of cycles to failure
N_b	number of blocks to failure
N_f	experimental number of cycles to failure
$N_{f,e}$	estimated number of cycles to failure
P_S	probability of survival
r	linear coordinate associated with the focus path
R	stress ratio
r_n	notch root radius
t	time instant
T_σ	scatter ratio of the endurance limit for 90% and 10% probabilities of survival
ΔK_{th}	threshold value of the stress intensity factor range
$\Delta\sigma$	range of the linear-elastic stress
$\Delta\sigma_A$	range of the plain fatigue/endurance limit
$\Delta\sigma_{nom}$	range of the nominal stress
ϕ	out-of-phase angle
ν	Poisson's ratio
ρ_{eff}	effective critical plane stress ratio
ρ_{lim}	intrinsic fatigue strength threshold
σ_A	fully-reversed uniaxial endurance limit at N_A cycles to failure
$\sigma_{n,a}$	amplitude of the stress perpendicular to the critical plane
$\sigma_{n,m}$	mean stress perpendicular to the critical plane
$\sigma_{n,max}$	maximum value of the stress perpendicular to the critical plane
$\sigma_{n,min}$	maximum value of the stress perpendicular to the critical plane
$\sigma_{0.2\%}$	0.2% proof stress
σ_{UTS}	ultimate tensile strength
Σ_a	amplitude of the nominal net axial stress
$\Sigma_{a,i}$	amplitude of the nominal net axial stress at the i-th stress level
$\Sigma_{a,max}$	maximum amplitude of the nominal net axial stress in the spectrum
Σ_m	mean value of the nominal net axial stress
$\Sigma_{m,max}$	maximum value of the nominal net mean axial stress in the spectrum
Σ_A	nominal net axial endurance limit at N_A cycles to failure
T_a	amplitude of the nominal net torsional stress
$\mathrm{T}_{a,i}$	amplitude of the nominal net torsional stress at the i-th stress level
$\mathrm{T}_{a,max}$	maximum amplitude of the nominal net torsional stress in the spectrum
T_m	mean value of the nominal net torsional stress
$\mathrm{T}_{m,max}$	maximum value of the nominal net mean torsional stress in the spectrum
T_A	nominal net torsional endurance limit at N_A cycles to failure
$\tau(t)$	time-variable shear stress
τ_a	shear stress amplitude relative to the critical plane
τ_A	fully-reversed torsional endurance limit at N_A cycles to failure
$\tau_{A,Ref}(\rho_{eff})$	fatigue strength at N_A cycles to failure
τ_m	mean shear stress relative to the critical plane
$\tau_{MV}(t)$	Resolved shear stress
$\tau_{MV,max}$	maximum value of the resolved shear stress
$\tau_{MV,min}$	minimum value of the resolved shear stress

1. Introduction

The emergence of additive manufacturing (AM), one of the most exciting and potentially transformative new manufacturing techniques, makes the need for understanding and modelling the fatigue behaviour of 3D-printed materials more pressing than ever. AM is *"the process of joining materials to make objects from 3D-model data, usually layer upon layer, as opposed to subtractive manufacturing methodologies"* (ASTM F42) and enables fabrication of complex designs which would be very challenging (if not impossible) using traditional technologies. Thanks to the advances in this rapidly evolving technological area, it is now possible to additively manufacture metals, polymers, composite materials, and concrete. Examination of the state of the art shows that, to date, researchers and industrialists have focussed their attention mainly on speeding up the process and on improving the overall quality of manufactured objects, thereby increasing the competitiveness of the technological process itself. However, examination of the state-of-the-art indicates that thus far our understanding of additively manufactured (AM) materials' mechanical/cracking behaviour under static, dynamic and fatigue loading is still at an initial stage, with this lack of in-depth knowledge somehow limiting exploitation of this powerful manufacturing technology.

Furthermore, whilst the potential for AM to disrupt conventional manufacturing processes has been widely recognised, its potential to be used to improve our fundamental understanding of the mode of structural response of components, structures and infrastructure has been much less widely appreciated – irrespective of manufacturing technique. For example, AM permits production of bespoke materials containing microstructural features specifically designed to maximise the reliability of measurement of specific predefined parameters, allowing research hypotheses to be tested robustly.

Turning to 3D-printed metallic materials, they can be additively manufactured by making use of very fine metal powders or wires that are melted by employing either a laser or an electron beam. Compared to the large variety of metals that can be manufactured using conventional processes, there is a limited choice of metallic materials that can be AM effectively. Common metals suitable for AM include Ti-based and Ni-based alloys as well as various stainless steel grades.

As far as AM metals are concerned, their overall fatigue behaviour is seen to be affected markedly by the complex material micro-/meso-/macro-structural features. In particular, in AM metals subjected to fatigue loading cracks are seen to initiate (due to Mode II governed mechanisms [1]) mainly from defects [2-6], where size, shape, orientation, location, and distribution of manufacturing flaws/voids play a role of primary importance [2-5, 7-9]. AM metals' fatigue strength is affected also by the specific features of the employed technology as well as by the values being adopted for the key manufacturing parameters/variables [2, 5, 6]. In this context, it is worth pointing out that, while orientation/elongation of grains, bonding between adjacent rows/layers and internal residual stresses certainly affect the overall fatigue performance of AM metals [2, 4, 6], the effect of the raster angle can be somehow mitigated by adopting specific post-manufacturing treatments [2]. Another important aspect is that fatigue lifetime of AM metallic materials depends also on the surface finishing, where strength can be enhanced markedly by using specific post-fabrication processes [1, 2, 5, 6].

Turning to the fatigue behaviour of AM metals containing geometrical features, much experimental evidence suggests that fatigue strength depends not only on the severity of the notch, but also on the manufacturing direction [10-12], with the crack initiation process being influenced by the existing interactions between sub-surface defects and local stress distributions [13]. In this context, it is interesting to observe that, very often, cracks are seen to initiate away from the notch tip, with this depending on the specific characteristics of the AM process being adopted [10-12]. Finally, it is worth recalling that, in the presence of stress raisers as well, notch fatigue strength of AM metals appears to be influenced markedly by the level of roughness characterising the surface in the stress concentration region [13-16].

Focussing attention on the fatigue assessment problem, it is important to observe that recent investigations strongly support the idea that the critical plane concept is successful also in estimating the strength of AM metallic materials subjected to multiaxial fatigue loading, with this holding true not only under constant, but also under variable amplitude load histories [5, 15, 17].

Finally, as far as notches are concerned, much experimental evidence suggests that material length scale parameters are successful in taking into account the detrimental effect of local stress concentration phenomena also in AM metals when they are subjected to fatigue loading [7, 10].

Taking as a starting point the body of knowledge briefly reviewed above, the present investigation attempts (for the first time) to extend the use of the Modified Wöhler Curve Method (MWCM) applied along with the Theory of Critical Distances (TCD) [18] to the fatigue assessment of notched AM steel subjected to complex multiaxial loading paths. In this setting, to check the accuracy and reliability of the design approach being proposed, a large number of new experimental data were generated by testing plain and notched specimens of AM AISI 316L. This comprehensive experimental investigation was run under both constant and variable amplitude multiaxial fatigue loading, with this being done by assessing the effect not only of non-zero mean stresses, but also of in-phase and out-of-phase load histories.

2. Stress quantities relative to the critical plane according to the Shear Stress-Maximum Variance Method.

As it will be reviewed briefly in the next section, the MWCM is a bi-parametrical multiaxial fatigue criterion that makes use of the critical plane concept. In this setting, the critical plane is defined as that material plane (passing through the assumed critical point – i.e., point O in Fig. 1a) which experiences the maximum amplitude of the shear stress, τ_a [19, 20].

In order to use the MWCM to assess multiaxial fatigue lifetime of AM components, in the present investigation the stress quantities relative to the critical plane are suggested to be calculated by taking full advantage of the Shear Stress-Maximum Variance Method (τ-MVM) [21-23]. As per Fig. 1a, the use of the τ-MVM is based on the assumption that the critical plane coincides with that material plane containing the direction, **MV**, which is associated with the maximum variance of the resolved shear stress, $\tau_{MV}(t)$ [22-24]. Having determined the orientation of the critical plane based on direction **MV**, it is straightforward to define also normal direction **n** which is the direction perpendicular (at point O) to the critical plane itself (Fig. 1a). As soon as directions **MV** and **n** are known, they can be used to calculate the shear stress quantites and the normal stress quantities, respectively, associated with the critical plane under investigation. In particular, the definitions suggested here as being employed in situations of practical interest are summarised in Fig. 2b and in Fig. 2c for the case of constant amplitude (CA) and variable amplitude (VA) load histories, respectively [25, 26].

According to the definitions summarised in Fig. 2c, under VA load histories the equivalent amplitude of the shear stress relative to the critical plane is calculated by simply post-processing the shear stress resolved along direction **MV**. The fact that, by definition, $\tau_{MV}(t)$ is a monodimensional stress quantity allows the cycle counting under VA fatigue loading to be performed directly, with this holding true independently of the degree of multiaxiality and non-proportionalty of the load history being assessed. In particular, as shown in Fig. 2d, monodimensional time-variable stress signal $\tau_{MV}(t)$ can be post-processed effectively and unambigously by simply using the classic Rain-Flow counting method [25]. By so doing, the cycles being counted allow the corresponding shear stress spectrum to be built directly (Fig. 2d).

The definitions briefly reviewed in the present section will be used in what follows not only to recall the main features of the MWCM, but also to post-process the experimental results we generated by testing plain and notched specimens of AM AISI316L.

3. Fundamentals of the MWCM under CA and VA fatigue loading

As mentioned at the beginning of the previous section, the MWCM is a multiaxial fatigue criterion that assesses fatigue damage via the shear and normal stress components relative to the plane of maximum shear stress amplitude [18-20]. This plane is usually referred to as the critical plane. The MWCM lays its theoretical foundations on the effective critical plane stress ratio, ρ_{eff}, that is defined as follows [27]:

$$\rho_{eff} = \frac{m \cdot \sigma_{n,m}}{\tau_a} + \frac{\sigma_{n,a}}{\tau_a} \tag{1}$$

In definition (1) $\sigma_{n,m}$, $\sigma_{n,a}$ and τ_a are the mean normal stress, the normal stress amplitude and the maximum shear stress amplitude relative to the critical plane, respectively. Material constant m is the mean stress sensitivity index. m ranges between 0 and 1 [27] and can be determined from suitable experimental results [18]. Accordingly, ρ_{eff} allows the effect of non-zero mean stress to be taken into account explicitly. Further, thanks to the way it is defined, stress ratio ρ_{eff} is capable of modelling not only the degree of multiaxiality, but also the degree of non-proportionality of the load history being applied [18-20].

The core concept on which the MWCM is based is explained schematically via the modified Wöhler diagram seen in Fig. 2. This log-log chart plots the shear stress amplitude relative to the critical plane, τ_a, against the number of cycle to failure, N_f. In accordance with the schematisation shown in Fig. 2, as far as conventional metallic materials are concerned, the modified Wöhler curves are seen to shift downward in the modified Wöhler diagram as stress ratio ρ_{eff} increases [18-20]. In terms of modelling, any modified Wöhler curve in the chart of Fig. 2 is described unambiguously through the negative inverse slope, $k_\tau(\rho_{eff})$, and the reference shear stress endurance limit, $\tau_{A,Ref}(\rho_{eff})$, at N_A cycle to failure. Based on this theoretical framework whose validity is fully supported by the experimental evidence [18-20, 25, 27], the hypothesis can be formed that relationships $k_\tau(\rho_{eff})$ and $\tau_{A,Ref}(\rho_{eff})$ are to be formulated explicitly by simply using two linear functions, i.e. [19, 20]:

$$k_\tau(\rho_{eff}) = (k - k_0) . \rho_{eff} + k_0 \qquad \text{for } \rho_{eff} \leq \rho_{lim} \tag{2}$$

$$\tau_{A,Ref}(\rho_{eff}) = \left(\frac{\sigma_A}{2} - \tau_A\right) \cdot \rho_{eff} + \tau_A \qquad \text{for } \rho_{eff} \leq \rho_{lim} \tag{3}$$

In Eqs (2) and (3) k and σ_A are the negative inverse slope and the endurance limit (extrapolated at N_A cycles to failure) describing the fully-reversed uniaxial fatigue curve (ρ_{eff}=1). Similarly, k_o and τ_A are the negative inverse slope and the endurance limit (again extrapolated at N_A to failure) associated with the torsional fatigue curve (ρ_{eff}=0). In definitions (2) and (3) ρ_{lim} is an intrinsic fatigue strength threshold that can be determined experimentally [27]. This fatigue strength threshold is used to model those situations characterised by very large values of ρ_{eff} [28]. In particular, these load histories are assessed by simply taking, in governing equations (2) and (3), the negative inverse slope and the reference shear stress amplitude equal to the corresponding values that can be estimated by setting ρ_{eff} invariably equal to ρ_{lim} [18, 27].

Having estimated via Eqs (2) and (3) a suitable modified Wöhler curve to be used to quantified fatigue damage, lifetime under CA cyclic loading can directly be predicted as follows [20] (Fig. 2):

$$N_{f,e} = N_A \cdot \left[\frac{\tau_{A,ref(\rho_{eff})}}{\tau_a}\right]^{k_\tau\,(\rho_{eff})} \tag{4}$$

where ρ_{eff} and τ_a are the critical plane stress ratio and the maximum shear stress amplitude relative to the critical plane, respectively, that are associated with the CA loading path under investigation.

Turning to VA situations, the procedure to be followed to use the MWCM to estimate fatigue lifetime is described in Fig. 3 [25]. In particular, by post-processing the time-variable stress state at superficial point O (Fig. 3a), the τ-MVM can be used to determine the orientation of the critical plane via the direction, **MV**, experiencing the maximum variance of the resolved shear stress. From stress signals $\tau_{MV}(t)$ and $\sigma_n(t)$ the relevant stress quantities relative to the critical plane can be calculated (Figs 3b and 3c) according to the definitions summarised in Fig. 1c. τ_a, $\sigma_{n,a}$ and $\sigma_{n,m}$ allow then the critical plane stress ratio, ρ_{eff}, to be estimated directly (Fig. 3d). As soon as ρ_{eff} is known, its value can then be used to estimate, via Eqs (2) and (3), the values of $k_\tau(\rho_{eff})$ and $\tau_{A,Ref}(\rho_{eff})$ associated with the modified Wöhler curve to be used to estimate fatigue damage according to the MWCM (Figs 3d and 3e).

Having determined a suitable fatigue design curve, shear stress signal $\tau_{MV}(t)$ can now be post-processed according to the Rain-Flow counting method [29] (Fig. 3f) to build the corresponding shear stress spectrum (Fig. 3g). This load spectrum together with Palmgren and Miner's rule [30, 31] (Fig. 3h) can now be used to estimate the total damage associated with the VA load history under investigation, i.e.:

$$D = \sum_{i=1}^{j} \frac{n_i}{N_{f,i}} \tag{5}$$

Finally, having quantified the extent of the total damage, the number of blocks, N_b, and cycles, $N_{f,e}$, to failure is estimated directly as follows (Fig. 3i):

$$N_b = \frac{D_{cr}}{D} = \frac{D_{cr}}{\sum_{i=1}^{j} \frac{n_i}{N_{f,i}}};\ N_{f,e} = \frac{D_{cr}}{D} \sum_{i=1}^{j} n_i \tag{6}$$

where D_{cr} is the critical value of the damage sum.

With regard to D_{cr}, according to the theory due to Palmgren [30] and Miner [31], failure under VA fatigue loading is supposed to occur as soon as D becomes equal unity, i.e., $D_{cr}=1$ in Eqs (6). However, as far as conventional metallic materials are concerned, the experimental value of D_{cr} is seen to vary in the range 0.02-10 [32]. In this context, it is important to observe that much experimental evidence suggests that, for a given conventional metallic material, D_{cr} varies not only as the geometry of the component being assessed varies (notch geometry and notch sharpness included), but also as profile, degree of multiaxiality and level of non-proportionality of the assessed load history change [32, 33]. Accordingly, the fact that D_{cr} is affected, amongst other parameters, by sharpness/profile of the stress concentrator being designed is an intrinsic limitation of Palmgren and Miner's theory, with this drawback being expected to somehow affect also our approach's overall accuracy. In this setting, owing to the fact that the international scientific community has not yet agreed on a commonly accepted theory suitable for estimating D_{cr} theoretically, running appropriate experiments still represents the only way to determine the critical value of the damage sum in a reliable and rigorous way.

If attention is focused specifically on the MWCM, D_{cr} can be estimated experimentally according to relationships (6) [45]. In particular, by running a series of experiments under given variable amplitude load histories, the number of cycles to failure can be determined for the various specimens being tested. Therefore, owing to the fact that $N_{f,e}$ is now the known experimental parameter, D_{cr} in relationships (6) becomes the un-known variable and it can be quantified directly via the calibration results themselves. This should make it evident that the experimental procedure to be followed to estimate D_{cr} in Eqs (6) is the same as the one commonly used to quantify the critical value of the damage sum according to the standard stress based approach [32].

The final aspect that is important to consider here is the way the modified Wöhler curves can be re-adjusted in order to effectively account for the damage extent associated with cycles of small stress amplitude. In particular, as recommended by Haibach [34], the negative inverse slope of the modified Wöhler curves is suggested to be taken, in the high-cycle fatigue regime (i.e., for $N_f>N_{kp}$ in Fig. 3e), equal to $m_\tau(\rho_{eff})=2k_\tau(\rho_{eff})-1$ [25]. This assumption will be used in what follows to post-process the experimental results generated by testing notched AM specimens of AISI316L under VA multiaxial fatigue loading.

4. Simplifying assumptions to apply the TCD to assess AM metallic materials

According to the definition due to David Taylor [35], the Theory of Critical Distances (TCD) is an umbrella covering a number of design approaches that all make use of specific length scale parameters to assess the strength of materials containing geometrical features of all kinds. As far as high-cycle notch fatigue strength is concerned, the first formalisations of the TCD were proposed halfway through the last century by Neuber [36] and Peterson [37] who formulated the Line Method and the Point Method, respectively.

After the advent of Linear Elastic Fracture Mechanics, the TCD was further developed [38, 39] and the critical distance to be used to perform the high-cycle fatigue assessment of cracked/notched components was proposed to be estimated as follows [38-40]:

$$L = \frac{1}{\pi}\left(\frac{\Delta K_{th}}{\Delta \sigma_A}\right)^2 \quad (7)$$

In definition (7) ΔK_{th} is the threshold value of the stress intensity factor range and $\Delta\sigma_A$ is the range of the plain fatigue (or endurance) limit. Since, according to Eq. (7), the critical distance is calculated via two material properties, L is in turn a material property, but its value changes as the applied load ratio, $R=\sigma_{min}/\sigma_{max}$, varies [35].

The TCD can be used also to perform the fatigue assessment in the finite life regime [41, 42], with this being done by still using a linear-elastic constitutive law to model the mechanical behaviour of the material being assessed. To this end, the definition used for the material characteristic length must be re-adjusted to take into account the fact that, in the medium-cycle fatigue regime, the critical distance value is seen to increase as the number of cycles to failure decreases [41]. This experimental evidence can be taken into account by simply modelling the critical distance via a power law, i.e. [41, 42]:

$$L_M = A \cdot N_f^B \quad (8)$$

In Eq. (8) A and B are two fatigue constants that can be estimated, for a specific material under a specific load ratio, from the plain fatigue curve and a fatigue curve determined experimentally by testing specimens weakened by a notch with known profile [41]. Fig. 4 summarises the strategy that is suggested here as being followed to estimate fatigue constants A and B in Eq. (8). In particular, assume that the critical distance value is to be estimated for a number of cycles to failure equal to $N_{f,i}$. According to Fig. 4a, $\Delta\sigma$ is the stress range breaking the plain material at $N_{f,i}$ cycles to failure. In a similar way, $\Delta\sigma_{nom}$ is the nominal stress range breaking the material containing the known geometrical feature again at $N_{f,i}$ cycles to failure (Fig. 4a). According to the Point Method (PM) [35], half of the critical distance, i.e., $L_M(N_{f,i})/2$, is equal the distance from the notch tip at which the local linear elastic stress perpendicular to the notch bisector equals the stress which breaks the plain material at $N_{f,}=N_{f,i}$ (Fig. 4b). By using this simple strategy, the critical distance can then be estimated for any number of cycles to failure, with the calculated values for L_M allowing constants A and B to be determined unambiguously.

As far AM titanium alloys are concerned, in a recent investigation [43] it has been proven experimentally that, under uniaxial fatigue loading, the variation of L_M in the medium-cycle fatigue regime is so limited that it can be neglected, with this simplifying assumption resulting just in a little loss of accuracy. In the present investigation, this hypothesis is attempted to be extended also to the multiaxial fatigue assessment of AM AISI 316L, where L, Eq. (7), is estimated in the high-cycle fatigue regime. Therefore, in the next section the procedure to apply the MWCM along with the PM will be reformulated in order to incorporate into our design approach this simplifying assumption.

To conclude, it is worth observing that either changing the AM metallic material, changing the AM technology being adopted, or, for a given AM process, changing the values of the manufacturing parameters may result in a critical distance value that varies with N_f as observed in conventional metallic materials. If this were the case, it is expected that the MWCM can still be applied along with the TCD to perform the fatigue assessment, provided that this design methodology is used along with critical distance (8), i.e., in its standard form [41, 42, 44-46].

4. The MWCM used along with the PM to assess notched AM metallic materials under CA and VA load histories

The simplified procedures being proposed in the present investigation to be followed to apply the MWCM in conjunction with the PM to estimate fatigue lifetime of notched AM components are summarised in Figs 5 and 6 for the case of CA and VA multiaxial fatigue loading, respectively.

As per the graphic flow-charts reported in these two figures, the first step is to estimate the linear-elastic stress distribution along the focus path. In this context, the focus path is defined as a straight line that emanates from the assumed crack initiation location (point A) and is normal to the surface at the hot spot itself (Figs 5a and 6a). As soon as the time-variable linear-elastic stress field in the highly stressed region is known, the subsequent step is to determine the state of stress at critical point O. According to the PM, point O belongs to the focus path and its distance from the notch tip is equal to L/2 (Figs 5a and 6a). Subsequently, the time-variable stress tensor at critical point O is to be post-processed according to the τ-MVM in order to determine the orientation of the critical plane (Figs 5b and 6b) as well as the associated stress quantities, i.e., τ_a, $\sigma_{n,m}$ and $\sigma_{n,a}$ (Fig. 5c and Figs 6c and 6d). Given the values for τ_a and ρ_{eff} being calculated, the resulting Modified Wöhler curve is then estimated from governing equations (2) and (3) that are directly calibrated through the parent (i.e., un-notched) material fatigue properties (Figs 5d and 5e and Figs 6e and 6f).

Having derived the modified Wöhler curve to be used to estimate fatigue damage, as far as CA time-variable loading is concerned, lifetime can be estimated directly via Eq. (4) – see Fig. 5e.

To perform the fatigue assessment under VA loading instead, the procedure described in Fig. 3 must be applied in conjunction with the PM as shown in Fig. 6. In particular, initially, resolved shear stress $\tau_{MV}(t)$ is post-processed (Figs 6c and 6g) to determine the corresponding resolved shear stress spectrum (Fig. 6h). Subsequently, the cycles being counted via the Rain-Flow method together with Palmgren and Miner's rule (Fig. 6f) are used to estimate the total damage associated with the VA load history under investigation (Fig. 6i). Lastly, having quantified total damage D, the number of blocks/cycles to failure is estimated directly through Eq. (6) – see Fig. 6k, where, again, D_{cr} is the critical value of the damage sum.

Having formulated a simplified approach to use the MWCM along with the PM to perform the multiaxial fatigue assessment of notched AM metallic materials, the next step is to assess the accuracy of the procedures described in Figs 5 and 6 against suitable experimental results. This will be done in the next sections.

5. Experimental results, post-processing of raw data, and cracking behaviour

The specimens of 316L stainless steel used in the present investigation were additively manufactured by employing the Selective Laser Melting (SLM) technology. The parent material was 3D-printed by setting the laser power equal to 450W, the scan speed to 1500-2000 mm/s, and the scan pitch to 0.05 mm. The final geometries of the specimens were fabricated from rods that were additively manufactured flat on the build plate. Before being machined using a conventional lathe, the 3D-printed rods were annealed. In this post-AM heat-treatment process, the temperature was set equal to 490 °C and the heating time to 6 hours, with the cooling process being based on argon. The technical drawings of the plain and notched specimens that were fabricated according to the above protocol are reported in Fig. 7. It is worth pointing out here that particular care was taken in order to reach, in the critical regions, the level of surface finishing as indicated in the drawings of Fig. 7.

Static and fatigue tests were run in the laboratories of Nanjing University of Aeronautics and Astronautics, China, by using a MTS 809 axial/torsional testing machine.

The post-heat treatment static properties of the AM stainless steel being investigated were experimentally determined to be as follows: Young's modulus, E, equal to 190.8 GPa, Poisson's ratio, ν, to 0.3, 0.2% proof stress, $\sigma_{0.2\%}$, to 380 MPa, and ultimate tensile strength, σ_{UTS}, to 642 MPa.

The CA and VA axial/torsional fatigue tests were run under force/moment control. The experimental number of cycles to failure, N_f, was defined as the number of cycles required to initiate and propagate visible technical cracks having length approximately equal to 1 mm.

The experimental results generated under CA fatigue loading are summarised in Tabs 1 to 4, with the meaning of the adopted symbols being explained in the nomenclature.

The VA fatigue tests were run by employing the concave upwards spectrum with sequence length equal to 1000 cycles that is summarised in Tab. 5. This spectrum was built by referring to a conventional Rayleigh distribution. In Tab. 5, $\Sigma_{a,i}$ and $T_{a,i}$ are used to denote, at the i-th stress level, the amplitude of the nominal net axial stress and the amplitude of the nominal net torsional stress, respectively. $\Sigma_{a,max}$ is the maximum amplitude of the nominal net axial stress in the spectrum, whereas $T_{a,max}$ is the maximum amplitude of the nominal net torsional stress in the same spectrum.

The experimental results generated by testing both plain and notched specimens under fatigue loading are summarised in Tab. 6, where, again, the meaning of the adopted symbols is explained in the nomenclature.

Due to the high cost of the individual specimens, the run-out samples were all re-tested, with the re-used specimens being clearly marked in Tabs 1 to 4 as well as in Tab. 6.

The raw data being generated under CA fatigue loading were initially re-analysed by assuming a log-normal distribution of the number of cycles to failure for each stress level, with a confidence level of 95% [47, 48]. The results from the statistical re-analyses are summarised in Tab. 7 in terms of out-of-phase angle (ϕ), load ratio (R), negative inverse slope (k), nominal net axial endurance limit (Σ_A), nominal net torsional endurance limit (T_A), and, finally, scatter ratio, T_σ, of the endurance limit for 90% and 10% probabilities of survival. As recommended by the International Institute of Welding for welded metals [49], the endurance limits reported in Tab. 7 were extrapolated at $N_A=2\cdot10^6$ cycles to failure for a probability of survival, P_S, equal to 50%. Lastly, it is worth observing that, according to Tab. 7, for the AM AISI 316 L stainless steel under investigation the fully-reversed uniaxial plain endurance limit, σ_A, was determined to be equal to 249 MPa (for P_S=50%), whereas the fully-reversed torsional plain endurance limit, τ_A, to 216.1 MPa (for P_S=50%).

As far as the AM AISI 316 L stainless steel under investigation is concerned, according to both the raw data reported in Tabs 1 to 4 and the values from the statistical re-analyses summarised in Tab. 7, it is possible to come to the following conclusions:

- fatigue strength is seen to decrease as the sharpness of the notch increases;
- irrespective of specimen geometry, the presence of non-zero mean stresses lowers AM AISI316L's overall fatigue strength;
- in the absence of notches, the effect of an out-of-phase angle equal to 90º is very little;
- in the presence of stress concentration phenomena, a 90º out-of-phase angle has a beneficial effect under R=-1, whereas it has a (slightly) detrimental effect under R=0.

In terms of observed cracking behaviour, the direct inspection of the fracture surfaces revealed that the crack initiation process took place mainly on the surface of the specimens, with this holding true independently of stress concentration level as well as of degree of multiaxiality and non-proportionality of the applied CA/VA load history. However, in a limited number of cases, some fatigue cracks were seen to initiate also from small sub-surface defects that were introduced during the AM process. It is important to observe here also that, in the notched specimens, the fatigue cracks were seen to emanate always from the notch tip region. In other words, contrary to what was observed by Solberg and Berto [10, 11], in the presence of stress concentration phenomena the crack initiation process never took place away from the notch apices themselves - i.e., away from those geometrical points experiencing the largest magnitude of the local linear-elastic stresses. This is a consequence of the fact that the geometrical features being tested were all machined by using a conventional lathe (after heat-treating the parent AM rods) and not 3D-printed directly.

As far as the cracking behaviour is concerned, in the specimens being tested the crack initiation process was seen to be mainly Mode II-dominated (i.e., a conventional Stage I crack initiation mechanism). In particular, irrespective of type of loading path and specimen's geometry, initiation and early stage propagation of fatigue cracks were seen to occur on those materials planes experiencing the maximum shear stress amplitude. This is fully confirmed by the pictures reported in Fig. 8 that show some examples of the cracks observed in the plain specimens subjected to fully-reversed axial as well as to fully-reversed torsional fatigue loading. In particular, Figs 8a to 8d show that, under axial loading, the cracks initiated on planes at about 45° to the specimen axis. In contrast, Figs 8e to 8h makes it evident that, under torsional loading, the fatigue cracks were seen to initiate on planes that were either parallel or perpendicular to the specimen axis. Independently of the type of loading, the Stage II process was seen to be mainly Mode I governed, with conventional branching occurring under cyclic torsion. These considerations regarding the cracking behaviour strongly support the idea that the critical plane concept is the right tool to be used to attempt to model the fatigue behaviour of the AM AISI 316L stainless steel under investigation.

6. Validation

In order to validate the proposed approach against the fatigue data being generated, the first step was calibrating the MWCM. According to the experimental results generated by testing the plain specimens under axial (both with R=-1 and R=0) as well as under fully-reversed torsional cyclic loading (Tabs 1 and 7), the relevant fatigue constants in governing equations (2) and (3) were calculated to be as follows (with $N_A=2\cdot10^6$ cycles to failure) [18]:

$$\sigma_A=249 \text{ MPa}, k=15.3 \ (P_S=50\%, R=-1) \tag{9}$$

$$\tau_A=216.1 \text{ MPa}, k_0=32.7 \ (P_S=50\%, R=-1) \tag{10}$$

$$m=0.53, \rho_{lim}=1.45 \tag{11}$$

The experimental, N_f, vs. estimated, $N_{f,e}$, number of cycles to failure diagram reported in Fig. 9a summarises the overall accuracy of the MWCM in assessing the fatigue strength of the plain specimens being tested. This diagram confirms that our multiaxial fatigue damage parameter is successful in modelling the fatigue behaviour of the AM AISI 316L stainless steel under investigation, with this holding true irrespective of degree of multiaxiality and degree of non-proportionality of the applied CA loading path. In particular, the error diagram of Fig. 9a demonstrates that the MWCM is capable of estimates falling within the largest scatter band amongst those associated with the three fatigue curves used for calibration. This outcome is certainly satisfactory, since it is unrealistic to expect a predictive methodology to result in estimates that are less scattered than the calibration data set itself. Turning to the plain fatigue results generated under uniaxial fully-reversed VA fatigue loading, the error chart of Fig. 9a confirms that estimates characterised by an acceptable level of accuracy were obtained by simply taking the critical value of the damage sum, D_{cr}, invariably equal to unity [30, 31].

Having calibrated the MWCM and then checked its accuracy against those data generated by testing the plain samples, the subsequent step was post-processing the results from the notched specimens. The linear-elastic stress fields in the notch tip regions needed to apply the TCD in the form of the PM were determined, through commercial software ANSYS®, by solving simple axisymmetric Finite

Element (FE) models, where the density of the mapped mesh was refined gradually until convergence has occurred.

Initially, the solutions from the linear-elastic FE analyses were used to estimate critical distance L, Eq. (7). In particular, since the experimental value for ΔK_{th} was not available, L was directly estimated at $N_A=2\cdot10^6$ cycles to failure according to the procedure shown in Fig. 4 [41, 50]. This was done by post-processing the fully-reversed plain fatigue curve and the fully-reversed uniaxial fatigue curve generated by testing the sharp notches (r_n=0.07 mm). This simple approach returned a value for the high-cycle fatigue critical distance, L, equal to 0.44 mm.

In terms of validation, the first exercise being performed aimed at checking the accuracy of the MWCM applied along with the PM in estimating notch endurance limits under CA multiaxial fatigue loading. According to the modified Wöhler diagram sketched in Fig. 2 as well as to Eq. (3), an engineering material is supposed to be at its fatigue/endurance limit as long as the following condition is assured [19, 27]:

$$\tau_a \leq \tau_{A,Ref}(\rho_{eff}) = \left(\frac{\sigma_A}{2} - \tau_A\right) \cdot \rho_{eff} + \tau_A \Rightarrow$$

$$\tau_a + \left(\tau_A - \frac{\sigma_A}{2}\right) \cdot \rho_{eff} \leq \tau_A \qquad \text{for } \rho_{eff} \leq \rho_{lim} \tag{12}$$

$$\tau_a + \left(\tau_A - \frac{\sigma_A}{2}\right) \cdot \rho_{lim} \leq \tau_A \qquad \text{for } \rho_{eff} > \rho_{lim} \tag{13}$$

Eqs (12) and (13) were then used together with the cyclic linear-elastic stress state at a distance from the notch tip equal to L/2 (Fig. 5) to build the τ_a vs. ρ_{eff} diagram seen in Fig. 9b. This diagram confirms that the MWCM applied along with the PM is successful in estimating the notch high-cycle fatigue strength of the AM stainless steel being tested. In particular, the systematic usage of the proposed approach to address the multiaxial notch endurance limit problem is seen to return estimates falling within an error interval of ±15%. This result is certainly satisfactory, especially in light of the fact that the TCD used to predict notch high-cycle fatigue strength of conventional metallic materials is seen to return estimates that fall within an average error interval of ±20% [51, 52].

Turning to the problem of estimating CA fatigue lifetime in the presence of stress concentrators, the modified Wöhler diagrams of Fig. 10 summarise the overall accuracy of the MWCM design curves in modelling the fatigue data that were determined experimentally by testing the notched specimens of AM AISI 316L. As per the design procedure summarised in Fig. 5, the relevant linear-elastic stress states were calculated, along the focus path, at a distance from the notch tip equal to L/2=0.22 mm. These time-variable stress states were then post-processed according to the τ-MVM in order to determine τ_a, $\sigma_{n,a}$, $\sigma_{n,m}$ and ρ_{eff}. The modified Wöhler diagrams of Fig. 10 confirm that the use of our approach resulted in estimates all characterised by an adequate level of accuracy. Solely the experimental results generated, in the low-cycle fatigue regime, by testing the sharply notched specimens under 90º out-of-phase loading with R=0 are seen to be slightly on the non-conservative side. However, in situations of practical interest, this would be easy to compensate via adequate design safety factors.

Finally, the experimental, N_f, vs. estimated, $N_{f,e}$, number of cycles to failure diagrams of Fig. 11 (together with the D_{cr} values reported in Tab. 6) summarise the overall accuracy of the MWCM/PM based design approach (Fig. 6) in estimating fatigue lifetime of notched AM AISI 316L under VA multiaxial fatigue loading. The error charts reported in Figs 11a, 11b and 11c were built by taking D_{cr} invariably equal to unity. Further, the calculations were done by correcting the slope of the modified Wöhler curves in the high-cycle fatigue regime as shown in Fig. 6f, with N_{kp} being taken equal to $2 \cdot 10^6$ cycles to failure.

The experimental critical values of the damage sum, $D_{cr,exp}$, listed in Tab. 6 confirm that the accuracy of the proposed approach (Figs 11a to 11c) is affected by the fact that $D_{cr,exp}$ varies in the range 0.04-465. In particular, $D_{cr,exp}$ is seen to depend on sharpness of the tested notch, degree of non-proportionality of the applied load history and load ratio. In this setting, the key problem associated with efficient assessment of notched AM metals under VA fatigue loading is that our capability of estimating $D_{cr,exp}$ is very limited due to a lack of specific scientific knowledge; indeed this applies to some extent to metallic materials in general [32, 53]. As far as AM metals are concerned, examination of the state of the art shows that, by and large, fatigue strength of 3D-printed stainless steel is seen to be influenced not only by the notch sharpness [10-12], but also by the combined effects of sub-surface defects and local stress distributions [13]. Accordingly, the existing interactions amongst these different variables may explain the reason why the AM metal considered in the present investigation was seen to be characterised by a very large variability in terms of $D_{cr,exp}$. In this context, it is worth observing that several attempts were made to post-process the notch VA results listed in Tab. 6 also by using other classic multiaxial fatigue criteria [54], with these approaches being applied along with the nominal stress based approach. The most relevant result from this validation exercise is that the $D_{cr,exp}$ values associated with the usage of these classic criteria were characterised by an even larger variability. This suggests that Palmgren and Miner's theory may not be the best one to assess the extent of damage under VA loading for the specific AM metal being considered in the present investigation.

However, despite the above difficulties, if the MWCM/PM (Fig. 6) is employed by adopting the average experimental values, $D_{cr,av}$, listed in Tab. 6, the use of the proposed design methodology returns predictions that are remarkably accurate, as demonstrated by the error chart of Fig. 11d. Accordingly, it is possible to conclude the present section by observing that more work needs to be done in the near future to formalise an approach capable of accurately estimating D_{cr} by taking into account geometry and specific features of the assessed VA load history, with this being done not only for AM, but also for conventional metallic materials.

6. Conclusions

The present paper summarises an attempt of reformulating the MWCM/PM-based design approach to make it suitable for designing notch components of AM AISI 316 L against CA and VA multiaxial fatigue loading. The accuracy and reliability of the design approach being proposed is validated by using a large number of experimental results. The most relevant conclusions are summarised in what follows.

- The fatigue strength of AM AISI 316L containing geometrical features is affected by notch sharpness, degree of multiaxiality and non-proportionality of the applied load history and magnitude of superimposed static stresses.
- In plain and notched specimens of AM AISI 316L, fatigue cracks were seen to initiate either on the surface or from sub-surface manufacturing defects.
- The crack initiation phase in the tested AM stainless steel was seen to be Mode II dominated. This conventional Stage I initiation mechanism was always followed by a Mode I governed Stage II process.

- According to the specific characteristics of the proposed fatigue design technique, the stress gradients in the highly stressed notch tip regions are assessed through the TCD applied in the form of the PM. The MWCM is used instead to account for the presence of superimposed static stresses as well as for the degree of multiaxiality and the non-proportionality of the applied load history.
- The proposed design methodology allows notched components of AM metallic materials to be designed against CA/VA uniaxial/multiaxial fatigue loading by directly post-processing the relevant stress fields determined via conventional linear-elastic FE models.
- The MWCM applied along with the τ-MVM and the PM is seen to be capable of predicting finite lifetime of notched AM metals subjected to CA/VA multiaxial fatigue loading by systematically reaching an adequate level of accuracy.
- More work needs to be done to formulate a robust approach allowing the critical value of the damage sum to be estimated as geometry of the component being assess and features of the VA load history under consideration vary.

Acknowledgment

Financial support for this project from the National Natural Science Foundation of China (Project No. 51875276) is gratefully acknowledged.

References

[1] Molaei R, Fatemi A, Phan N. Multiaxial fatigue of LB-PBF additive manufactured 17–4 PH stainless steel including the effects of surface roughness and HIP treatment and comparisons with the wrought alloy. Int J Fatigue 2020;137:105646

[2] Molaei R, Fatemi A, Phan N. Significance of hot isostatic pressing (HIP) on multiaxial deformation and fatigue behaviors of additive manufactured Ti-6Al-4V including build orientation and surface roughness effects. Int J Fatigue 2018;117:352–70.

[3] Yadollahi A et al. Fatigue life prediction of additively manufactured material: Effects of surface roughness, defect size, and shape. Fatigue Fract Eng Mater Struct 2018;41:1602–1614.

[4] Fatemi A et al. Fatigue behaviour of additive manufactured materials: An overview of some recent experimental studies on Ti-6Al-4V considering various processing and loading direction effects. Fatigue Fract Eng Mater Struct 2019;42:991–1009.

[5] Fatemi A, Molaei R, Phan N. Multiaxial fatigue of additive manufactured metals: Performance, analysis, and applications. Int J Fatigue 2020; 134:105479.

[6] Pegues JW et al. Fatigue of additive manufactured Ti-6Al-4V, Part I: The effects of powder feedstock, manufacturing, and post-process conditions on the resulting microstructure and defects. Int J Fatigue 2020;132:105358.

[7] Benedetti M, Santus C. Notch fatigue and crack growth resistance of Ti-6Al-4V ELI additively manufactured via selective laser melting: A critical distance approach to defect sensitivity. Int J Fatigue 2019;121:281–292.

[8] Karpenko O, Oterkus S, Oterkus E. Peridynamic investigation of the effect of porosity on fatigue nucleation for additively manufactured titanium alloy Ti6Al4V. Theor Appl Fract Mech 2021;112:102925

[9] Wang Y, Su Z. Effect of micro-defects on fatigue lifetime of additive manufactured 316L stainless steel under multiaxial loading. Theor Appl Fract Mech. 2021;111:102849.

[10] Solberg K, Berto F. Notch-defect interaction in additively manufactured Inconel 718. Int J Fatigue. 2019;122:35–45.

[11] Solberg K, Berto F. A diagram for capturing and predicting failure locations in notch geometries produced by additive manufacturing. Int J Fatigue. 2020;134:105428.

[12] Nicoletto G, Konečnab R, Frkanb M, Riva E. Influence of layer-wise fabrication and surface orientation on the notch fatigue behavior of as-built additively manufactured Ti6Al4V. Int J Fatigue. 2020;134:105483.

[13] Molaei R, Fatemi A, Phan N. Notched fatigue of additive manufactured metals under axial and multiaxial loadings, Part I: Effects of surface roughness and HIP and comparisons with their wrought alloys. Int J Fatigue. 2021;143:106003.

[14] Kahlin M, Ansell H, Moverare , JJ. Fatigue behaviour of notched additive manufactured Ti6Al4V with as-built surfaces. Int J Fatigue. 2017;101:51–60.

[15] Molaei R, Fatemi A. Fatigue performance of additive manufactured metals under variable amplitude service loading conditions including multiaxial stresses and notch effects: Experiments and modelling. Int J Fatigue. 2021;145:106002.

[16] Solberg K, Wan D, Berto F. Fatigue assessment of as-built and heat-treated Inconel 718 specimens produced by additive manufacturing including notch effects. Fatigue Fract Eng Mater Struct. 2020;43:2326–2336.

[17] Molaei R et al. Fatigue of additive manufactured Ti-6Al-4V, Part II: The relationship between microstructure, material cyclic properties, and component performance. Int J Fatigue 2020;132:105363

[18] Susmel L. Multiaxial Notch Fatigue: from nominal to local stress-strain quantities. Woodhead & CRC, Cambridge, UK, 2009.

[19] Susmel L, Lazzarin P. A Bi-parametric Modified Wöhler Curve for high cycle multiaxial fatigue assessment. Fatigue Fract Eng Mater Struct. 2002;25:63-78.

[20] Lazzarin P, Susmel L. A stress-based method method to predict lifetime under multiaxial fatigue loadings. Fatigue Fract Eng Mater Struct. 2003; 26:1171-1187.

[21] Susmel L, Tovo R, Benasciutti D. A novel engineering method based on the critical plane concept to estimate lifetime of weldments subjected to variable amplitude multiaxial fatigue loading. Fatigue Fract Eng Mater Struct. 2009; 32:441-459.

[22] Susmel L. A simple and efficient numerical algorithm to determine the orientation of the critical plane in multiaxial fatigue problems. Int J Fatigue. 2010;32:1875-1883.

[23] Luo P, Yao W, Susmel L. An improved critical plane and cycle counting method to assess damage under variable amplitude multiaxial fatigue loading. Fatigue Fract Eng Mater Struct. 2020;43:2024-2039.

[24] Susmel L, Tovo R, Socie DF. Estimating the orientation of Stage I crack paths through the direction of maximum variance of the resolved shear stress. Int J Fatigue. 2014;58:94–101.

[25] Susmel L, Tovo R. Estimating fatigue damage under variable amplitude multiaxial fatigue loading. Fatigue Fract Eng Mater Struct. 2011;34:1053-1077.

[26] Susmel L. Four stress analysis strategies to use the Modified Wöhler Curve Method to perform the fatigue assessment of weldments subjected to constant and variable amplitude multiaxial fatigue loading. Int J Fatigue. 2014;67;38-54.

[27] Susmel L. Multiaxial fatigue limits and material sensitivity to non-zero mean stresses normal to critical planes. Fatigue Fract Eng Mater Struct. 2008;31:295-309.

[28] Susmel L, Tovo R, Lazzarin P. The mean stress effect on the high-cycle fatigue strength from a multiaxial point of view. Int J Fatigue. 2005;27:928-43.

[29] Matsuishi M, Endo T. Fatigue of metals subjected to varying stress. Presented to the Japan Society of Mechanical Engineers, Fukuoka, Japan; 1968.

[30] Palmgren A. Die Lebensdauer von Kugellagern. Verfahrenstechnik. 1924;68:339–341.

[31] Miner MA. Cumulative damage in fatigue. J Appl Mech. 1945;67:AI59–64.

[32] Sonsino CM. Fatigue testing under variable amplitude loading. Int J Fatigue. 2007;29:1080-1089.

[33] Sonsino CM, Kueppers M. Multiaxial fatigue of welded joints under constant and variable amplitude loadings. Fatigue Fract Engng Mater Struct. 2001;24:309–327.

[34] Haibach, E. (1989) Betriebsfestigkeit—Verfahren und Daten zur Bauteilberechnung. VDI-Verlag GmbH, Düsseldorf, Germany.

[35] Taylor D. The Theory of Critical Distances: a new perspective in Fracture Mechanics. Elsevier, Oxford, UK, 2007.

[36] Neuber H. Theory of notch stresses: principles for exact calculation of strength with reference to structural form and material. Springer Verlag, Berlin, II Ed. 1958.

[37] Peterson RE. Notch Sensitivity. In: Sines G., Waisman J. L., Editors. Metal Fatigue. New York. McGraw Hill 1959;293-306.

[38] Tanaka K. Engineering formulae for fatigue strength reduction due to crack-like notches. Int J Fracture 1983;22:R39-R45.

[39] Taylor D. Geometrical effects in fatigue: a unifying theoretical model. Int. J. Fatigue 1999;21:413-420.

[40] El Haddad MH, Topper TH, Smith KN. Fatigue crack propagation of short cracks. J Engng Mater Tech. 1979;101:42-45.

[41] Susmel L, Taylor D. A novel formulation of the Theory of Critical Distances to estimate lifetime of notched components in the medium-cycle fatigue regime. Fatigue Fract Engng Mater Struct. 2007;30:567-581.

[42] Susmel L, Taylor D. The Theory of Critical Distances to estimate lifetime of notched components subjected to variable amplitude uniaxial fatigue loading. Int J Fatigue. 2011;33:900-911.

[43] Al Zamzami I, Razavi SMJ, Berto F, Susmel L. The Critical Distance Method to estimate the fatigue strength of notched additively manufactured titanium alloys. Procedia Structural Integrity. 2020;28:994-1001.

[44] Susmel L, Taylor D. The Modified Wöhler Curve Method applied along with the Theory of Critical Distances to estimate finite life of notched components subjected to complex multiaxial loading paths. Fatigue Fract Engng Mater Struct. 2008;31:1047-1064.

[45] Susmel L, Taylor D. A critical distance/plane method to estimate finite life of notched components under variable amplitude uniaxial/multiaxial fatigue loading. Int J Fatigue. 2012;38:7-24.

[46] Louks R, Gerin B, Draper J, Askes H, Susmel L. On the multiaxial fatigue assessment of complex three-dimensional stress concentrators. Int J Fatigue. 2014;63:2014.

[47] Anon. Standard Practice for Statistical Analysis of Linear or Linearized Stress-Life (S-N) and Strain-Life (ε-N) Fatigue Data. ASTM E739; 2015.

[48] Al Zamzami I, Susmel L. On the accuracy of nominal, structural, and local stress based approaches in designing aluminium welded joints against fatigue. Int J Fatigue 2017;101:137-158.

[49] Hobbacher A. Recommendations For Fatigue Design of Welded Joints and Components. IIW document XIII-2151-07/XV-1254-07, 2007.

[50] Susmel L, Taylor D. The Theory of Critical Distances as an alternative experimental strategy for the determination of K_{Ic} and ΔK_{th}. Eng Frac Mech. 2010;77:1492–1501.

[51] Taylor D, Wang G. The validation of some methods of notch fatigue analysis. Fatigue Fract Engng Mater Struct. 2000;23:387–394.

[52] Susmel, L., Taylor, D., Tovo, R., On the estimation of notch fatigue limits by using the Theory of Critical Distances: L, a0 and open notches. SDHM Struct Durab Health Monit. 2008;4(1):1-18.

[53] Murakami Y, Takagi, T, Wada K, Matsunaga H. Essential structure of S-N curve: Prediction of fatigue life and fatigue limit of defective materials and nature of scatter. Int J Fatigue 2021;146:106138.

[54] Papadopoulos IV, Davoli P, Gorla C, Filippini, M, Bernasconi A. A comparative study of multiaxial high-cycle fatigue criteria for metals. Int J Fatigue 1997;19(3);219-235.

List of Captions

Table 1. Summary of the experimental results generated by testing under CA fatigue loading plain specimens of AM AISI 316L.

Table 2. Summary of the experimental results generated by testing under CA fatigue loading the notched specimens of AM AISI 316L with root radius, r_n, equal to 0.07 mm.

Table 3. Summary of the experimental results generated by testing under CA fatigue loading the notched specimens of AM AISI 316L with root radius, r_n, equal to 2 mm.

Table 4. Summary of the experimental results generated by testing under CA fatigue loading the notched specimens of AM AISI 316L with root radius, r_n, equal to 5 mm.

Table 5. Rayleigh distribution-based concave upwards spectrum with sequence length equal to 1000 cycles used to run the fatigue tests under VA fatigue loading.

Table 6. Summary of the experimental results generated by testing under VA fatigue loading plain and notched specimens of AM AISI 316L.

Table 7. Fatigue curves determined from the results generated by testing under CA fatigue loading plain and notched specimens of AM AISI 316L.

Figure 1. Definitions to calculate the stress components relative to the critical plane (a) under both constant (b) and variable amplitude loading (c, d).

Figure 2. Modified Wöhler diagram and fatigue assessment under CA fatigue loading.

Figure 3. The MWCM to estimate lifetime under VA fatigue loading.

Figure 4. Procedure to estimate the material critical distance via two calibration fatigue curves.

Figure 5. MWCM applied along with the PM to estimate finite lifetime of notched AM components subjected to CA fatigue loading.

Figure 6. MWCM applied along with the PM to estimate finite lifetime of notched AM components subjected to VA fatigue loading.

Figure 7. Geometries of the tested specimens (dimensions in millimetres).

Figure 8. Figure 8. Examples of the cracking behavior observed in the plain specimens tested under fully-revered axial fatigue loading (a-d) as well as under fully-reversed torsional fatigue loading (e-h) – in the pictures, the longitudinal axis of the cylindrical specimens is horizontal.

Figure 9. Accuracy of the MWCM in estimating the fatigue lifetime of the tested plain specimens of AM AISI 316L – Ax=axial loading; T=torsion; Bi=biaxial loading; IPh=In-Phase; OoPh=Out-of-Phase (a); accuracy of the MWCM applied along the PM in estimating CA endurance limit in the presence of notches (b).

Figure 10. Accuracy of the MWCM applied along with PM in estimating the CA fatigue lifetime of the tested notched specimens of AM AISI 316 L (Bi=biaxial loading; IPh=In-Phase; OoPh=Out-of-Phase).

Figure 11. Accuracy of the MWCM applied along with PM in estimating the VA fatigue lifetime of the tested notched specimens of AM AISI 316 L (IPh=In-Phase; OoPh=Out-of-Phase).

Tables

Code	Σ_a *[MPa]*	Σ_m *[MPa]*	T_a *[MPa]*	T_m *[MPa]*	R	ϕ *[°]*	f *[Hz]*	N_f *[Cycles]*	Run Out	Re-tested
P03	320	0			-1		1	36576		
P04	320	0			-1		1	68555		
P06	250	0			-1		2	1043051		
P07	250	0			-1		5	1706842		
P08	280	0			-1		3	412342		
P09	280	0			-1		3	618798		
P10	370	0			-1		1	4426		
P12	370	0			-1		1	3342		
P13	200	200			0		5	301913		
P14	200	200			0		5	205515		
P15	250	250			0		2	78135		
P16	250	250			0		2	73638		
P17	160	160			0		8	2004951	●	
P18	180	180			0		8	857648		
P19	170	170			0		8	2005966	●	
P19	300	300			0		1	19596		●
P20	180	180			0		8	1998224	●	
P20	300	300			0		1	19496		●
P21			175	0	-1		5	2048693	●	
P21			220	0	-1		2	1248245		●
P22			220	0	-1		2	725325		
P23			240	0	-1		2	107185		
P24			240	0	-1		1	98958		
P25			230	0	-1		1	253198		
P26			230	0	-1		1	248347		
P27			255	0	-1		1	4850		
P28			255	0	-1		1	9924		
P29	230	0	132.8	0	-1	0	3	27722		
P31	220	0	127	0	-1	0	3	574909		
P30	230	0	132.8	0	-1	90	3	633473		
P32	220	0	127	0	-1	90	3	2000000	●	
P34	190	190	109.7	109.7	0	0	1	69511		
P36	175	175	101	101	0	0	2	155716		
P35	190	190	109.7	109.7	0	90	1	80828		
P37	175	175	101	101	0	90	2	160274		

Table 1. Summary of the experimental results generated by testing under CA fatigue loading plain specimens of AM AISI 316L.

Code	Σ_a [MPa]	Σ_m [MPa]	T_a [MPa]	T_m [MPa]	R	ϕ [°]	f [Hz]	N_f [Cycles]	Run Out	Re-tested
V-01	220	0			-1		5	91803		
V-02	220	0			-1		3	42955		
V-03	135	0			-1		5	2002710	●	
V-03	250	0			-1		1	43596		●
V-04	170	0			-1		5	1604731		
V-05	195	0			-1		5	1044071		
V-06	195	0			-1		5	486818		
V-07	270	0			-1		1	39189		
V-08	270	0			-1		1	25396		
V-09	155	0	89.5	0	-1	0	2	575494		
V-10	155	0	89.5	0	-1	0	5	2038392	●	
V-11	190	0	109.7	0	-1	0	5	400053		
V-12	138	0	79.7	0	-1	0	8	2005448	●	
V-13	230	0	132.8	0	-1	0	2	30101		
V-14	230	0	132.8	0	-1	0	2	22265		
V-15	190	0	109.7	0	-1	0	2	76709		
V-16	200	200	115.5	115.5	0	0	2	7924		
V-17	200	200	115.5	115.5	0	0	2	5928		
V-18	120	120	69.3	69.3	0	0	5	232778		
V-19	120	120	69.3	69.3	0	0	8	2007071	●	
V-20	120	120	69.3	69.3	0	0	8	2000000	●	
V-21	150	150	86.7	86.7	0	0	5	64657		
V-22	150	150	86.7	86.7	0	0	5	70912		
V-23	130	130	75.1	75.1	0	0	6	516411		
V-24	130	130	75.1	75.1	0	0	6	1342918		
V-12	230	0	132.8	0	-1	90	2	3189		●
V-19	230	0	132.8	0	-1	90	2	7493		●
V-25	190	0	109.7	0	-1	90	6	36165		
V-26	190	0	109.7	0	-1	90	6	101949		
V-27	155	0	89.5	0	-1	90	7	1970361		
V-28	155	0	89.5	0	-1	90	8	2000042	●	
V-28	200	200	115.5	115.5	0	90	2	4707		●
V-20	200	200	115.5	115.5	0	90	2	10142		●
V-29	150	150	86.7	86.7	0	90	5	14281		
V-30	150	150	86.7	86.7	0	90	5	22526		
V-31	130	130	75.1	75.1	0	90	6	939062		
V-32	130	130	75.1	75.1	0	90	8	21974		
V-33	130	130	75.1	75.1	0	90	8	54506		
V-34	120	120	69.3	69.3	0	90	8	847439		
V-35	120	120	69.3	69.3	0	90	8	2004041	●	

Table 2. Summary of the experimental results generated by testing under CA fatigue loading the notched specimens of AM AISI 316L with root radius, r_n, equal to 0.07 mm.

Code	Σ_a [MPa]	Σ_m [MPa]	T_a [MPa]	T_m [MPa]	R	ϕ [°]	f [Hz]	N_f [Cycles]	Run Out	Re-tested
R2-01	250	0	144.3	0	-1	0	2	98800		
R2-02	250	0	144.3	0	-1	0	2	137100		
R2-03	210	0	121.2	0	-1	0	5	437192		
R2-04	210	0	121.2	0	-1	0	5	199238		
R2-05	190	0	109.7	0	-1	0	8	670976		
R2-06	190	0	109.7	0	-1	0	8	479740		
R2-07	170	0	98.1	0	-1	0	8	1104294		
R2-08	270	0	155.9	0	-1	0	2	34714		
R2-09	250	0	144.3	0	-1	90	2	85106		
R2-10	250	0	144.3	0	-1	90	2	106112		
R2-11	210	0	121.2	0	-1	90	5	2110571	•	
R2-11	270	0	155.9	0	-1	90	2	37818		•
R2-12	210	0	121.2	0	-1	90	5	83159		
R2-13	190	0	109.7	0	-1	90	6	1576358		
R2-14	190	0	109.7	0	-1	90	6	2000000	•	
R2-14	270	0	155.9	0	-1	90	2	80727		•
R2-15	210	210	121.2	121.2	0	0	2	44537		
R2-16	210	210	121.2	121.2	0	0	2	44441		
R2-17	180	180	103.9	103.9	0	0	5	122489		
R2-18	180	180	103.9	103.9	0	0	5	148534		
R2-19	160	160	92.4	92.4	0	0	6	281725		
R2-20	160	160	92.4	92.4	0	0	6	409673		
R2-21	140	140	80.8	80.8	0	0	8	496374		
R2-22	210	210	121.2	121.2	0	90	2	79796		
R2-23	210	210	121.2	121.2	0	90	2	88002		
R2-24	180	180	103.9	103.9	0	90	5	160297		
R2-25	180	180	103.9	103.9	0	90	5	110791		
R2-26	160	160	92.4	92.4	0	90	6	266665		
R2-27	160	160	92.4	92.4	0	90	6	365875		
R2-28	140	140	80.8	80.8	0	90	8	2028005	•	

Table 3. Summary of the experimental results generated by testing under CA fatigue loading the notched specimens of AM AISI 316L with root radius, r_n, equal to 2 mm.

Code	Σ_a [MPa]	Σ_m [MPa]	T_a [MPa]	T_m [MPa]	R	ϕ [°]	f [Hz]	N_f [Cycles]	Run Out	Re-tested
R5-01	290	0	167.4	0	-1	0	2	86359		
R5-02	290	0	167.4	0	-1	0	2	55842		
R5-03	260	0	150.0	0	-1	0	5	157459		
R5-04	260	0	150.0	0	-1	0	5	900807		
R5-05	230	0	132.7	0	-1	0	6	574035		
R5-06	230	0	132.7	0	-1	0	6	2000112	●	
R5-07	200	0	115.4	0	-1	0	8	2032024	●	
R5-08	290	0	167.4	0	-1	90	2	205614		
R5-09	290	0	167.4	0	-1	90	2	2026378	●	
R5-10	260	0	150	0	-1	90	5	1339995		
R5-11	260	0	150	0	-1	90	5	2072946	●	
R5-12	315	0	181.9	0	-1	90	2	106169		
R5-13	315	0	181.9	0	-1	90	2	76098		
R5-14	290	0	167.4	0	-1	90	5	168979		
R5-15	260	260	150.1	150.1	0	0	2	17556		
R5-16	260	260	150.1	150.1	0	0	2	15954		
R5-17	230	230	132.8	132.8	0	0	4	41058		
R5-18	230	230	132.8	132.8	0	0	4	38522		
R5-19	190	190	109.7	109.7	0	0	6	211696		
R5-20	160	160	92.4	92.4	0	0	8	2000493	●	
R5-21	175	175	101	101	0	0	8	378650		
R5-22	170	170	98.1	98.1	0	0	8	926366		
R5-23	250	250	144.3	144.3	0	90	2	53063		
R5-24	250	250	144.3	144.3	0	90	2	43292		
R5-25	200	200	115.4	115.4	0	90	4	171612		
R5-26	200	200	115.4	115.4	0	90	4	106951		
R5-27	170	170	98.1	98.1	0	90	6	2009372	●	
R5-28	170	170	98.1	98.1	0	90	6	2001122	●	
R5-29	180	180	103.9	103.9	0	90	6	311831		
R5-30	180	180	103.9	103.9	0	90	6	544057		

Table 4. Summary of the experimental results generated by testing under CA fatigue loading the notched specimens of AM AISI 316L with root radius, r_n, equal to 5 mm.

Stress level	n_i [Cycles]	$\Sigma_{a,i}/\Sigma_{a,max}$ $T_{a,i}/T_{a,max}$
1	1	1.000
2	3	0.931
3	6	0.862
4	12	0.793
5	21	0.724
6	36	0.655
7	56	0.586
8	63	0.524
9	80	0.469
10	97	0.414
11	111	0.359
12	120	0.303
13	120	0.248
14	109	0.193
15	88	0.138
16	57	0.083
17	20	0.028

Table 5. Rayleigh distribution-based concave upwards spectrum with sequence length equal to 1000 cycles used to run the fatigue tests under VA fatigue loading.

Specimen Type	Code	$\Sigma_{a,max}$ *[MPa]*	$\Sigma_{m,max}$ *[MPa]*	$T_{a,max}$ *[MPa]*	$T_{m,max}$ *[MPa]*	R	ϕ *[°]*	f *[Hz]*	N_f *[Cycles]*	Run Out	Re-tested	$D_{cr,exp}$	$D_{cr,av}$
Plain	P_32	370	0			-1		3	884299		•	0.60	2.15
	P_38	420	0			-1		2	390668			1.85	
	P_39	390	0			-1		4	2000000	•		-	
	P_39	450	0			-1		2	291758		•	4.98	
Sharp notch, r_n=0.07 mm	V-35	250	0	144.3	0	-1	0	2	1075859		•	3.5	2.41
	V-36	225	0	129.9	0	-1	0	4	1344292			1.98	
	V-37	300	0	173.2	0	-1	0	4	135908			1.74	
	V-38	250	0	144.3	0	-1	90	6	237497			0.26	0.22
	V-39	300	0	173.2	0	-1	90	4	37981			0.17	
	V-40	225	0	129.9	0	-1	90	6	442733			0.22	
	V-41	225	225	129.9	129.9	0	0	6	224074			0.33	0.34
	V-42	260	260	150.1	150.1	0	0	4	90009			0.39	
	V-43	195	195	112.6	112.6	0	0	6	616374			0.30	
	V-44	225	225	129.9	129.9	0	90	6	60859			0.04	0.05
	V-45	260	260	150.1	150.1	0	90	4	32271			0.06	
	V-46	195	195	112.6	112.6	0	90	6	195294			0.04	
Intermediate notch, r_n=2 mm	R2-28	310	0	179	0	-1	0	4	1024976		•	101.5	126.8
	R2-29	350	0	202.1	0	-1	0	4	299613			152.1	
	R2-30	310	0	179	0	-1	90	6	514382			3.2	7.03
	R2-31	350	0	202.1	0	-1	90	4	411851			10.9	
	R2-32	270	270	155.9	155.9	0	0	4	280155			2.87	2.87
	R2-33	270	270	155.9	155.9	0	90	4	346975			0.90	0.83
	R2-34	225	225	129.9	129.9	0	90	6	1176119			0.77	
Blunt notch, r_n=5 mm	R5-06	410	0	236.7	0	-1	0	4	116170		•	464.7	368.8
	R5-07	350	0	202.1	0	-1	0	6	853236		•	245.2	
	R5-09	380	0	219.4	0	-1	0	6	352997		•	396.6	
	R5-11	410	0	236.7	0	-1	90	4	304987		•	18.3	14.3
	R5-20	350	0	202.1	0	-1	90	6	1617092		•	10.4	
	R5-27	380	0	219.4	0	-1	90	6	2000000	•	•	-	
	R5-27	350	350	202.1	202.1	0	0	4	71568		•	12.78	7.7
	R5-28	310	310	179	179	0	0	6	162525		•	7.03	
	R5-31	280	280	161.7	161.7	0	0	2	290170			3.82	
	R5-32	310	310	179	179	0	90	4	142594			0.40	0.35
	R5-33	280	280	161.7	161.7	0	90	6	282568			0.37	
	R5-34	250	250	144.3	144.3	0	90	6	529763			0.29	

Table 6. Summary of the experimental results generated by testing under VA fatigue loading plain and notched specimens of AM AISI 316L.

Specimen Type	**N. of Data**	**ϕ** *[°]*	**R**	**k**	**Σ_A** *[MPa]*	**T_A** *[MPa]*	**T_σ**
Plain	8	-	-1	15.3	249.0	-	1.147
	9	-	-1	32.7	-	216.1	1.062
	10	-	0	6.8	152.3	-	1.193
Sharp r_n=0.07 mm	9	-	-1	9.1	164.9	-	1.431
	7	0	-1	8.1	136.8	79.0	1.700
	6	90	-1	14.9	152.6	88.1	1.266
	9	0	0	9.1	107.2	61.9	1.591
	9	90	0	7.6	89.9	51.9	2.404
Intermediate r_n=2 mm	8	0	-1	6.7	157.7	91.1	1.285
	8	90	-1	7.3	162.6	93.9	1.869
	7	0	0	6.4	117.9	68.1	1.196
	7	90	0	4.7	105.8	61.1	1.311
Blunt r_n=5 mm	7	0	-1	9.8	210.6	121.6	1.668
	7	90	-1	13.7	248.5	143.4	1.146
	8	0	0	8.8	149.0	86.1	1.145
	8	90	0	6.3	135.8	78.4	1.362

Table 7. Fatigue curves determined from the results generated by testing under CA fatigue loading plain and notched specimens of AM AISI 316L.

Figures

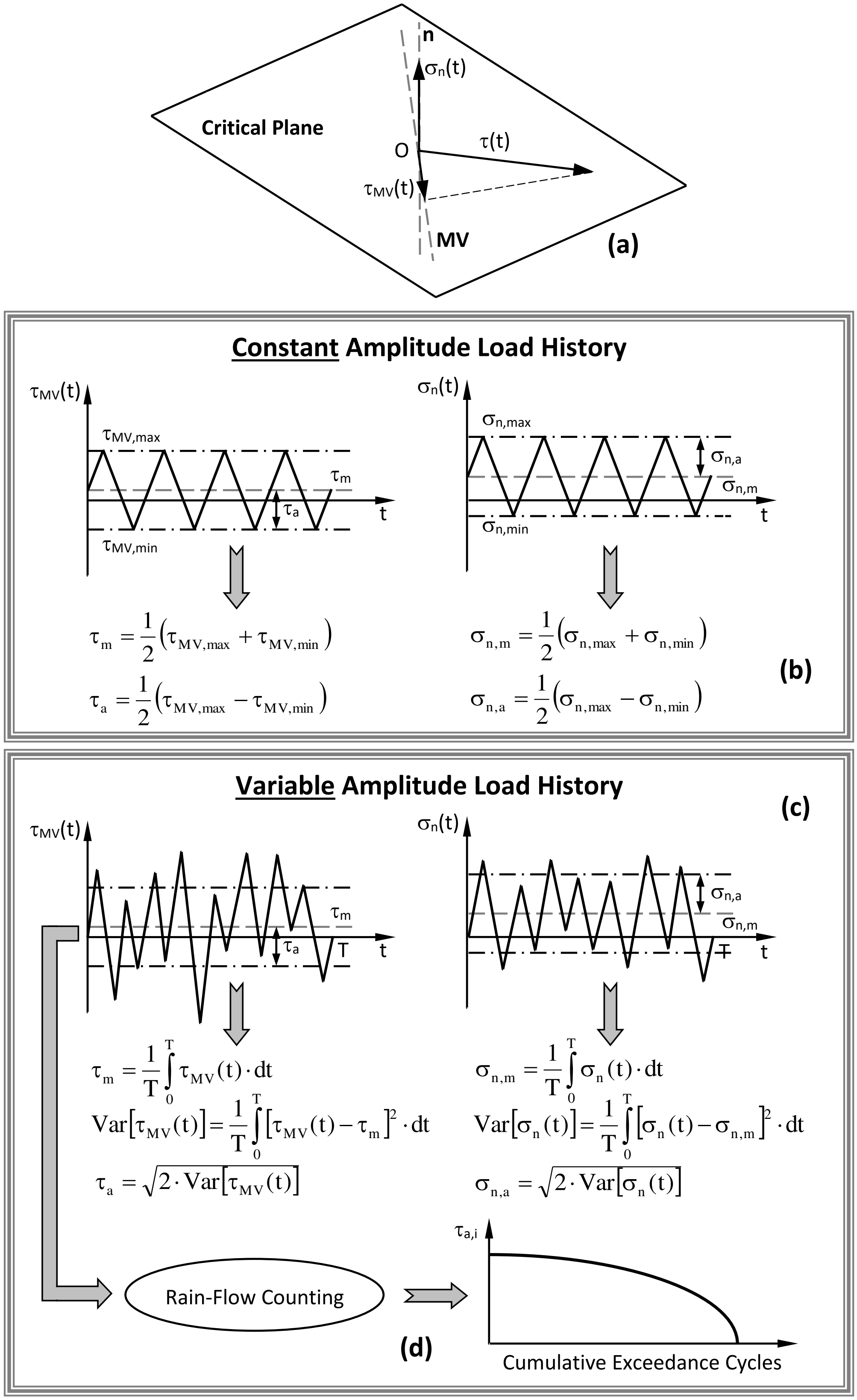

Figure 1: Definitions to calculate the stress components relative to the critical plane (a) under both constant (b) and variable amplitude loading (c, d).

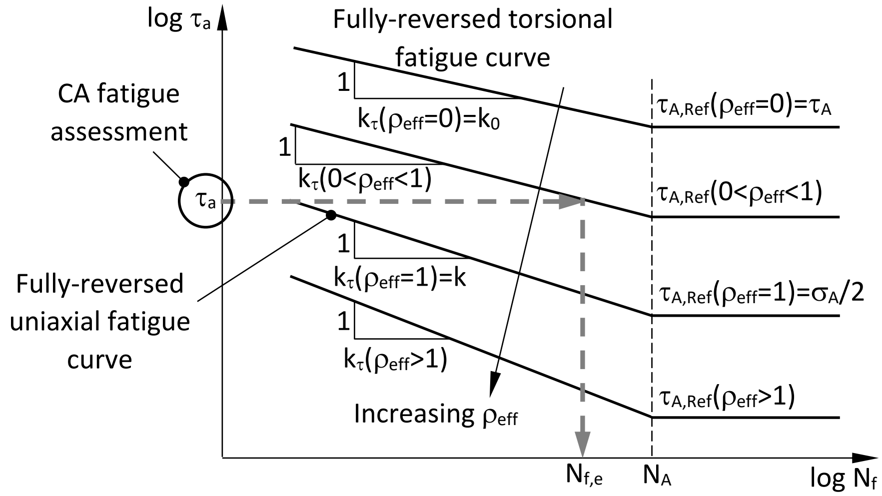

Figure 2. Modified Wöhler diagram and fatigue assessment under CA fatigue loading.

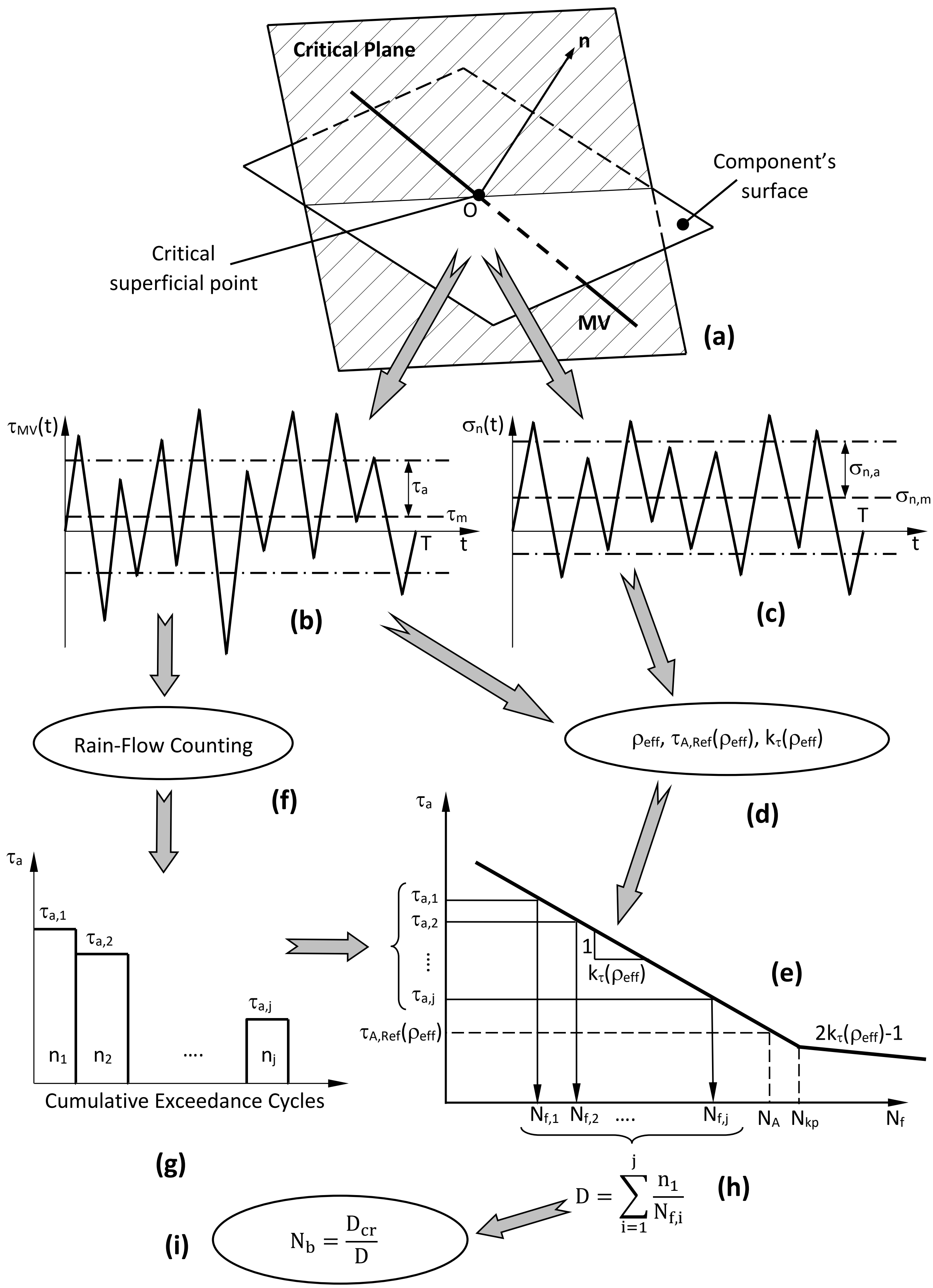

Figure 3. The MWCM to estimate lifetime under VA fatigue loading.

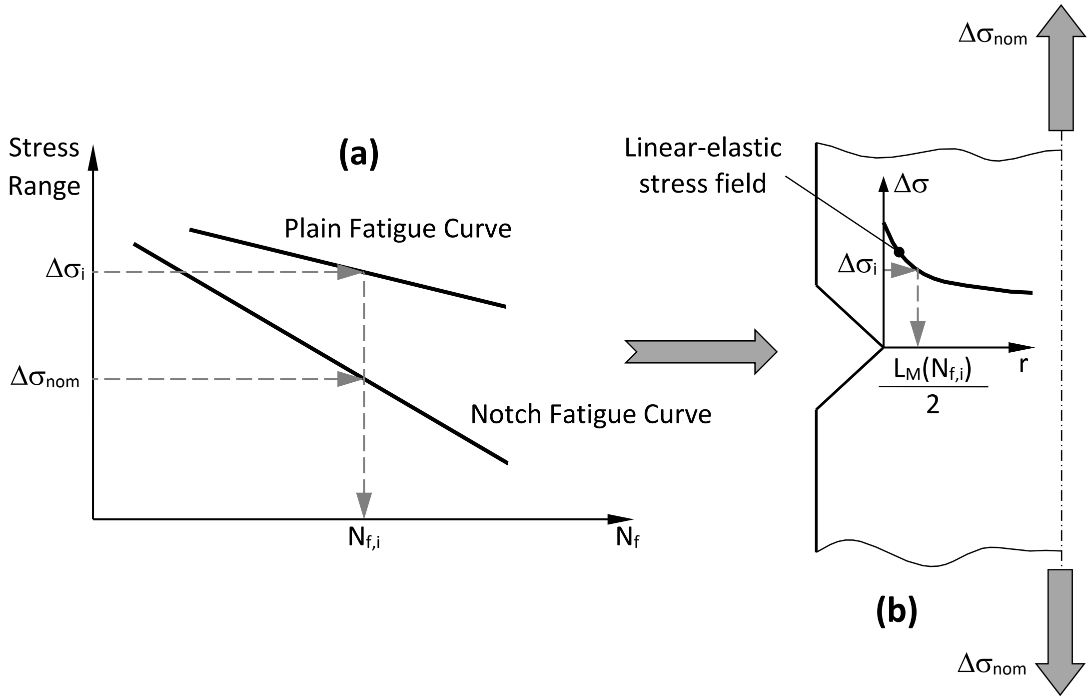

Figure 4. Procedure to estimate the material critical distance via two calibration fatigue curves.

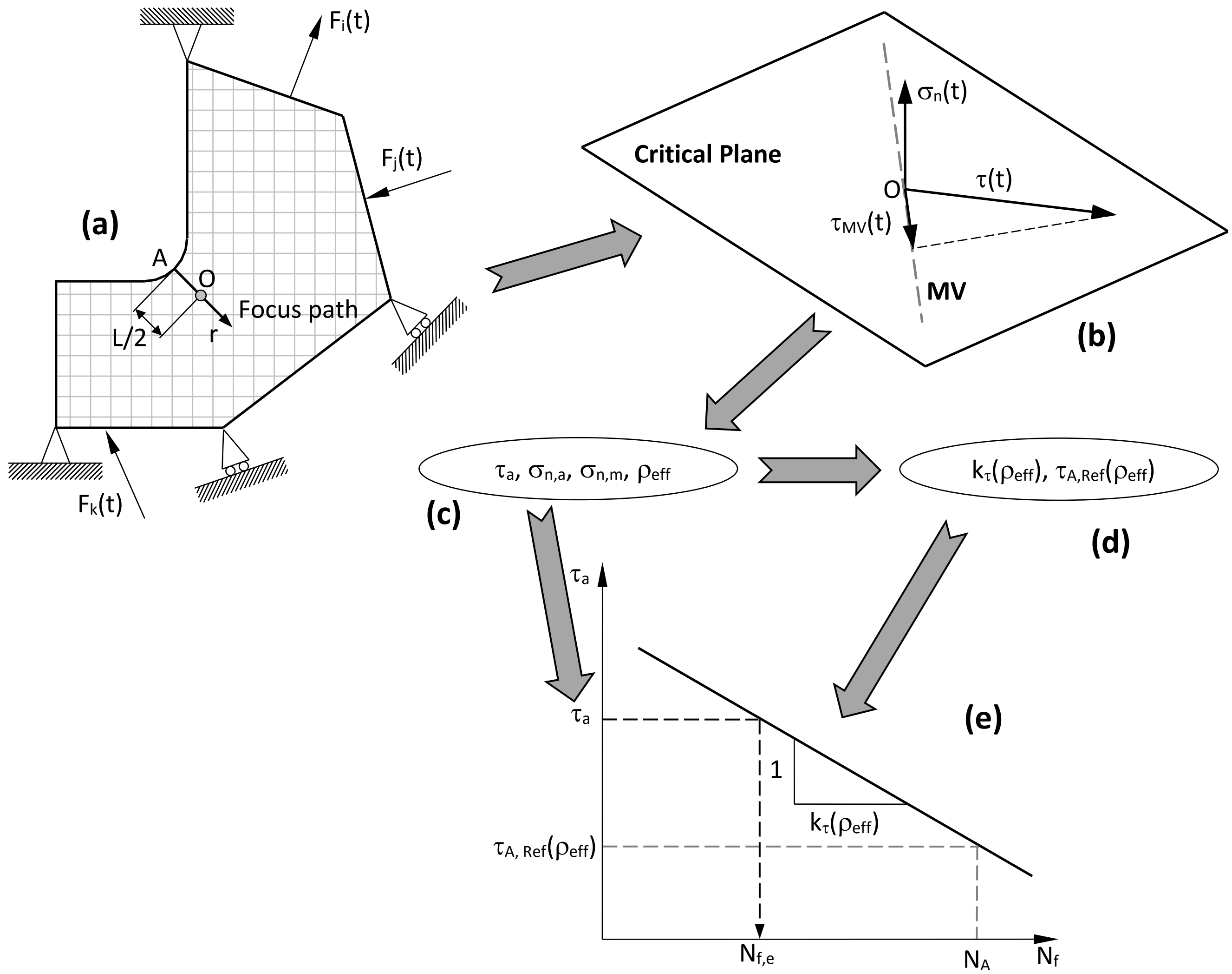

Figure 5. MWCM applied along with the PM to estimate finite lifetime of notched AM components subjected to CA fatigue loading.

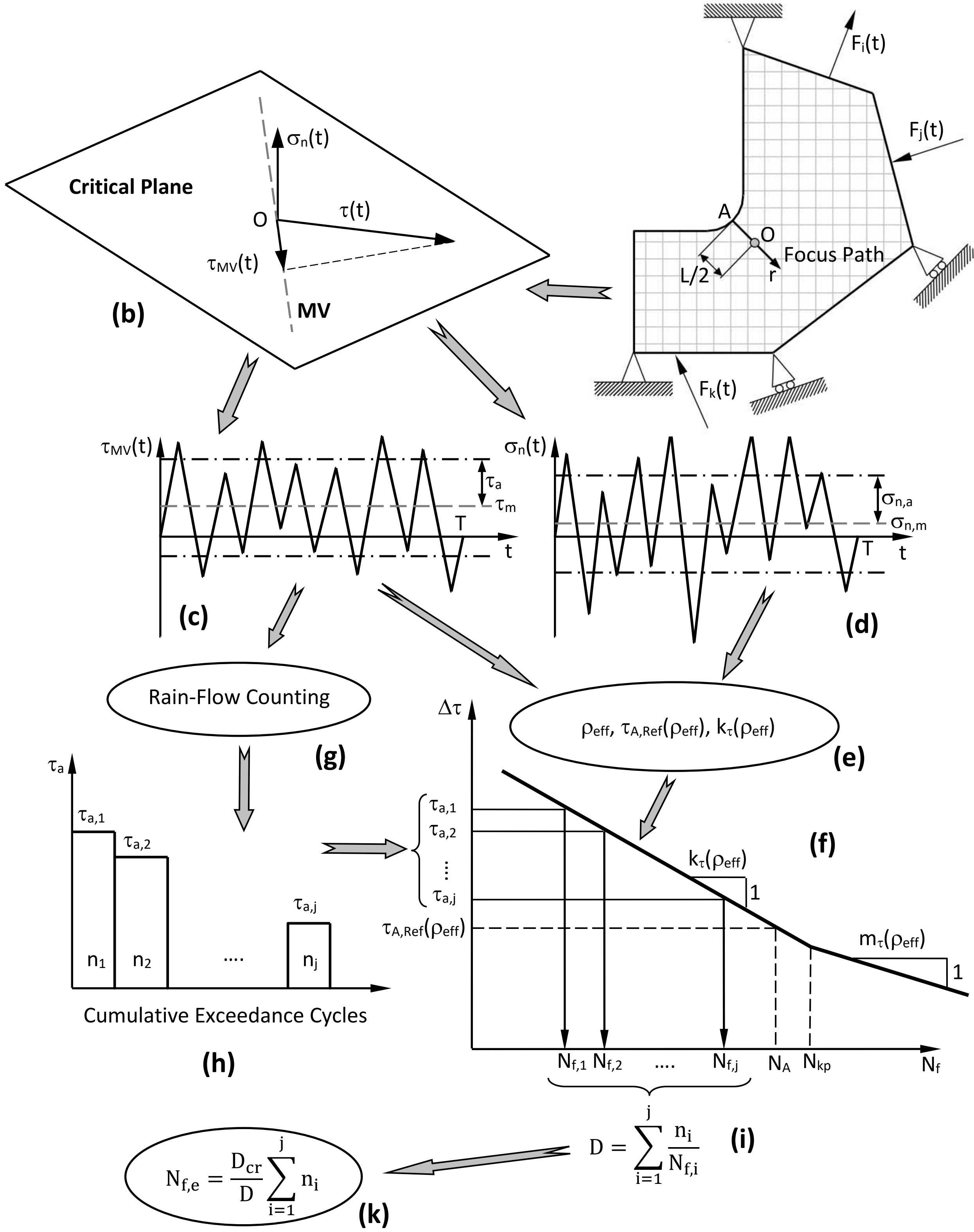

Figure 6. MWCM applied along with the PM to estimate finite lifetime of notched AM components subjected to VA fatigue loading.

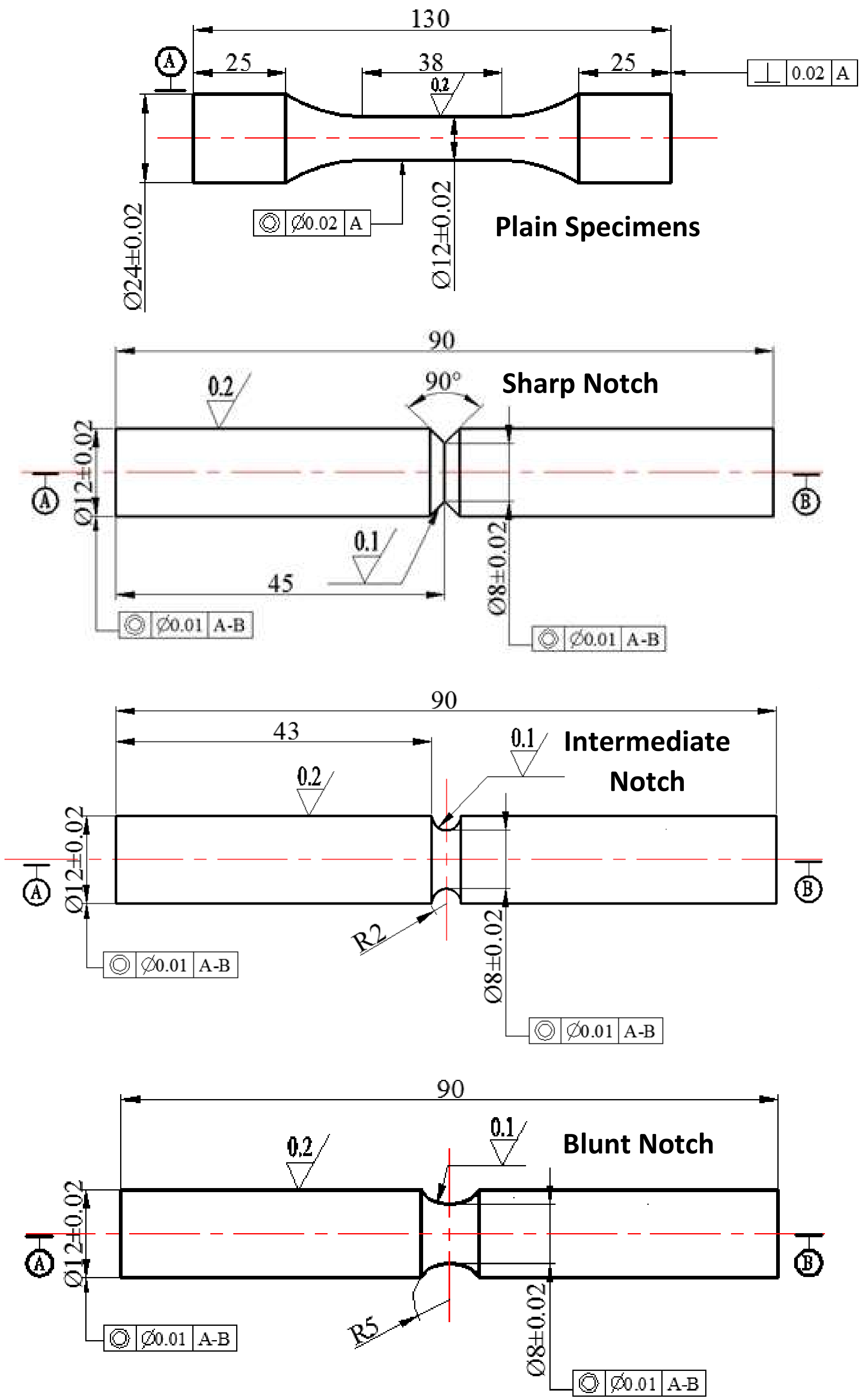

Figure 7. Geometries of the tested specimens (dimensions in millimetres).

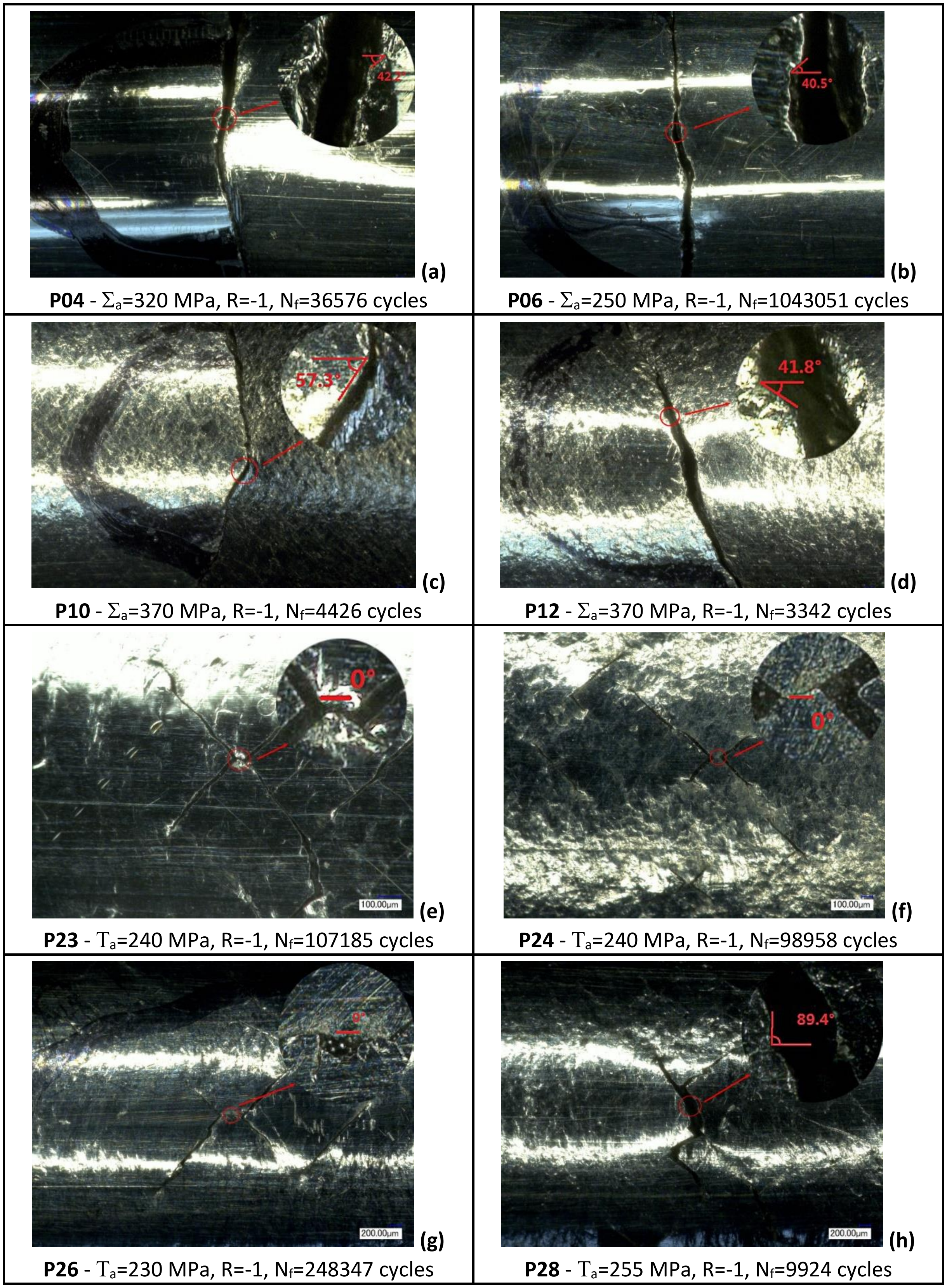

Figure 8. Examples of the cracking behavior observed in the plain specimens tested under fully-revered axial fatigue loading (a-d) as well as under fully-reversed torsional fatigue loading (e-h) – in the pictures, the longitudinal axis of the cylindrical specimens is horizontal.

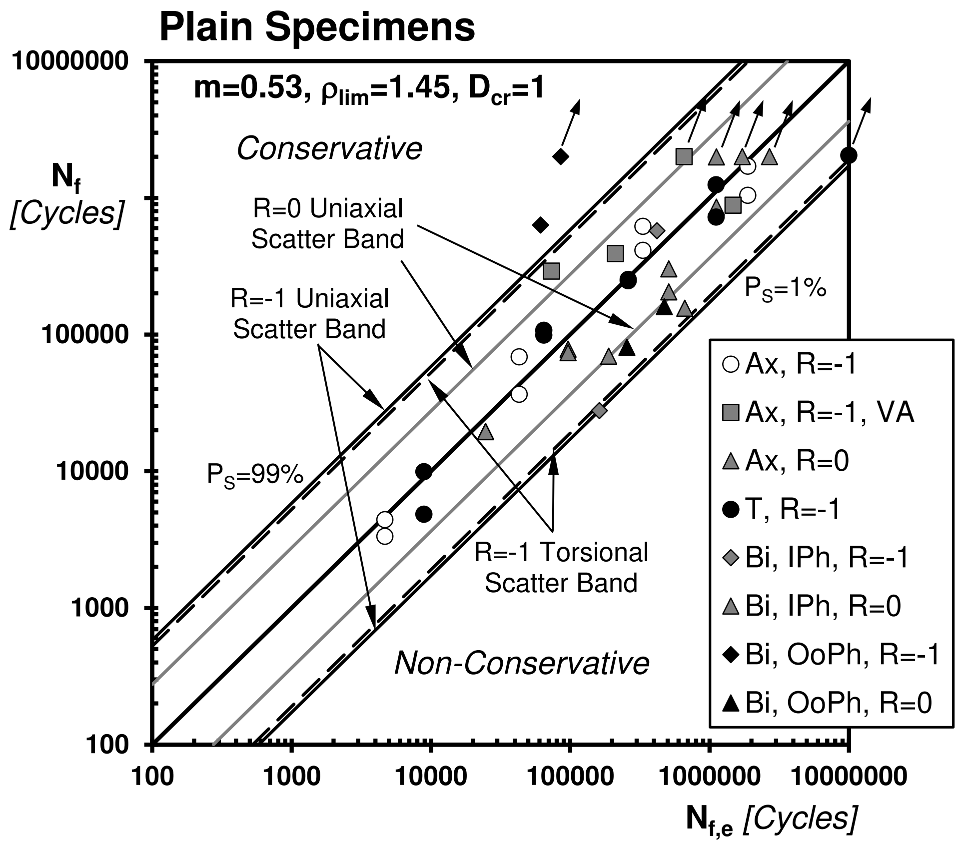

(a)

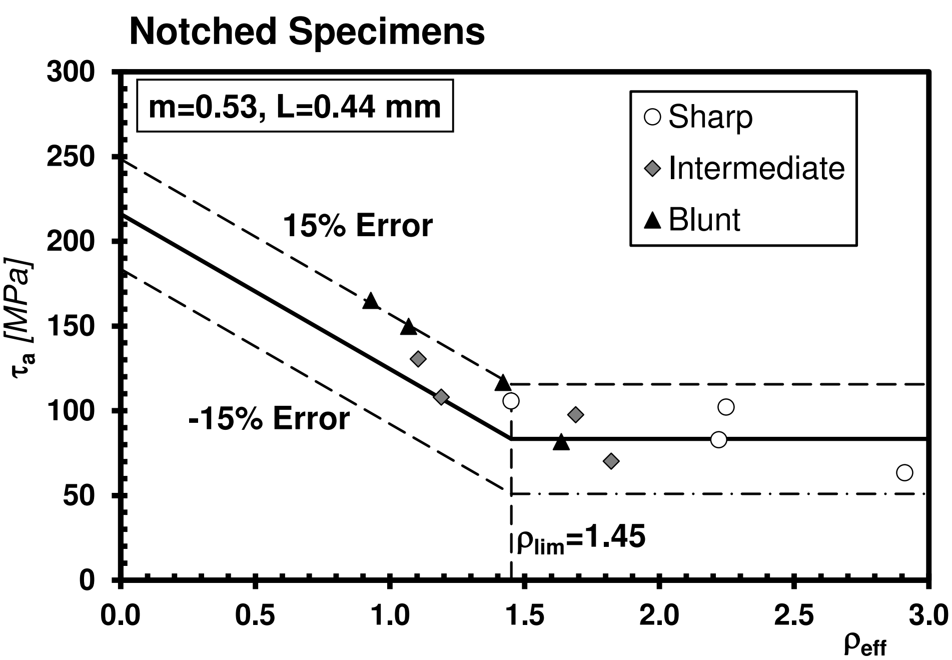

(b)

Figure 9. Accuracy of the MWCM in estimating the fatigue lifetime of the tested plain specimens of AM AISI 316L – Ax=axial loading; T=torsion; Bi=biaxial loading; IPh=In-Phase; OoPh=Out-of-Phase (a); accuracy of the MWCM applied along the PM in estimating CA endurance limit in the presence of notches (b).

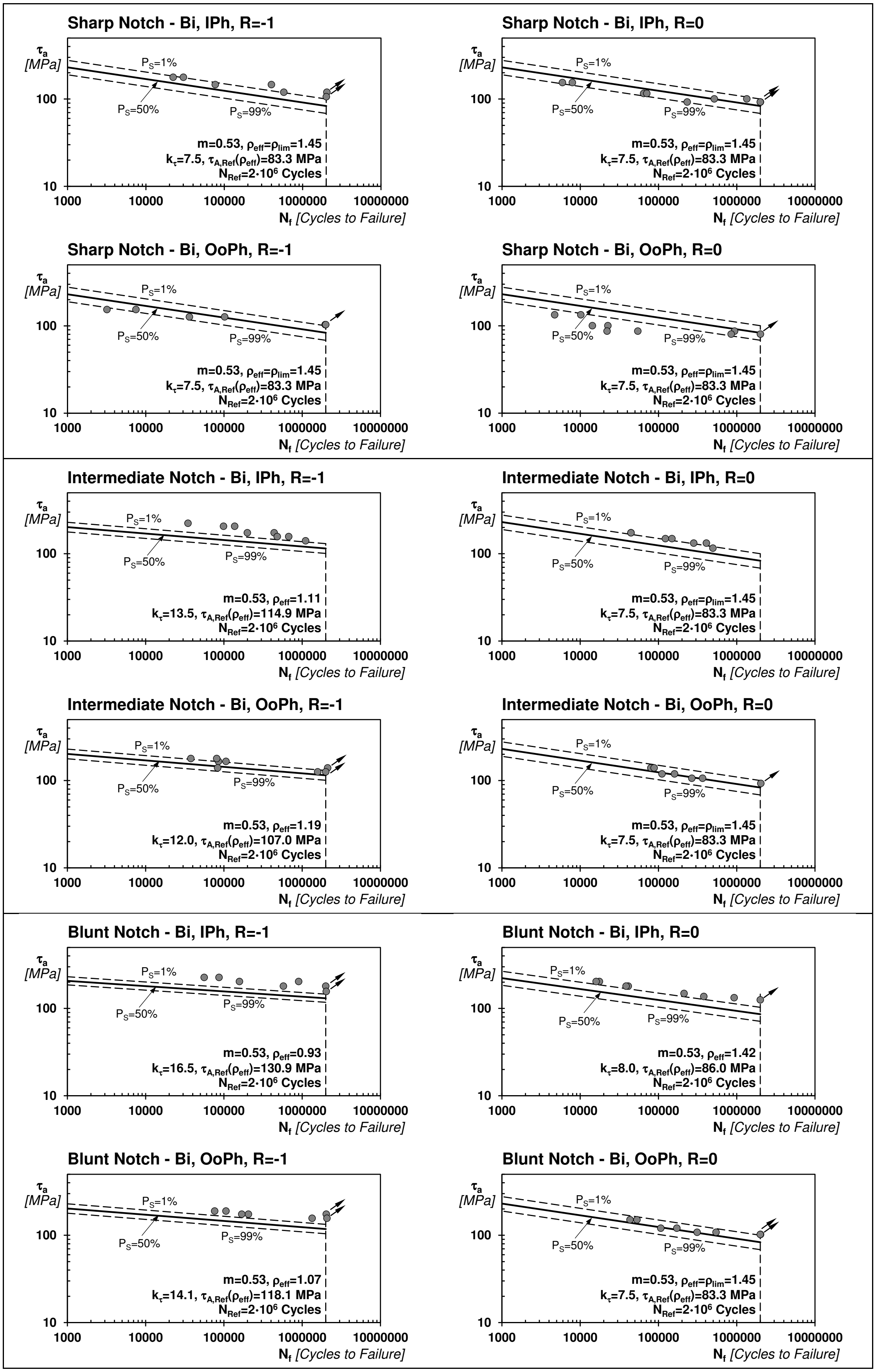

Figure 10. Accuracy of the MWCM applied along with PM in estimating the CA fatigue lifetime of the tested notched specimens of AM AISI 316 L (Bi=biaxial loading; IPh=In-Phase; OoPh=Out-of-Phase).

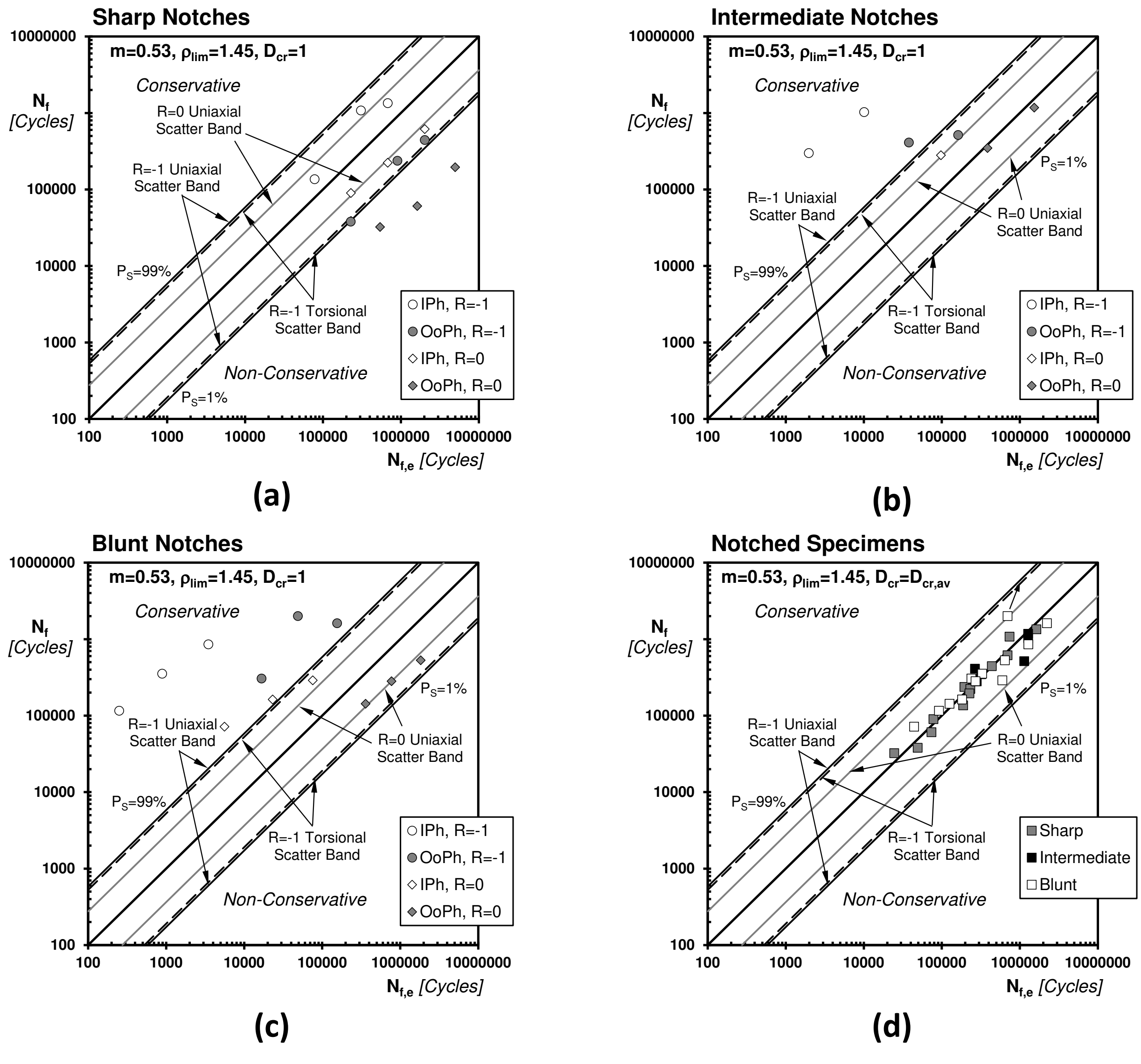

Figure 11. Accuracy of the MWCM applied along with PM in estimating the VA fatigue lifetime of the tested notched specimens of AM AISI 316 L (IPh=In-Phase; OoPh=Out-of-Phase).